Spatially coherent oscillations in neural fields with inhibition and adaptation. II. Two-dimensional domains

Stefanos E. Folias*

Department of Mathematics & Statistics, University of Alaska Anchorage, Anchorage, Alaska 99508, USA

(Received 4 November 2024; revised 18 September 2025; accepted 12 November 2025; published 8 January 2026)

We study the bifurcation of stationary activity bumps to localized, spatially coherent oscillations in a family of elementary neural field models involving nonlocal synaptic excitation and inhibition with Heaviside firing rate nonlinearity and local linear adaption, both with and without a localized input inhomogeneity, on two-dimensional spatial domain $\mathbb{R}^2$, including two cases of interacting pairs of neural fields. [We treat the same neural fields on the one-dimensional spatial domain $(-\infty, \infty)$ separately.] A general framework is constructed to analyze stationary bump solutions in a neural field model containing N neural fields with M linear gating variables that modulate different neural fields. A main focus is to demonstrate how underlying symmetries in this family of equations give rise to a related set of spatially coherent time-periodic solutions that bifurcate via Hopf bifurcation with respect to different spatial eigenmodes, each with different spatial structures being selected as a result of the relative balance of synaptic inhibition to excitation. A Hopf bifurcation with O(2) symmetry for radially symmetric stationary bumps is relevant for bifurcation with respect to higher-order spatial modes in these neural fields due to the geometric multiplicity of these eigenvalues resulting from the symmetries of the synaptic connections and input inhomogeneity. Hopf bifurcation of stationary bumps in these neural fields thereby produce either *breather* (standing wave) type of solutions with D_n dihedral symmetry or *rotor* (rotating wave) type of solutions with Z_n rotational symmetry when a stationary bump destabilizes in a supercritical Hopf bifurcation. Interacting pairs of symmetric neural fields that support bumps lead to different types of *in-phase* and *antiphase* breather and rotor solutions when stationary bumps destabilize in a Hopf bifurcation with respect to different eigenmodes. Stability of ring solutions is also studied and Hopf bifurcation is found to lead to different ring breathers and ring rotors with analogous n-fold symmetry. Secondary and subcritical bifurcations also occur in these neural fields on two-dimensional domains which can produce a diverse set of spatiotemporal patterns, particularly in the presence of an input inhomogeneity; however, this is beyond the scope of this study and will be treated in more depth separately.

DOI: 10.1103/kms3-vfgp

I. INTRODUCTION

Neural field equations are nonlocal partial integrodifferential equations that describe the average activity in large populations of neurons on spatial domains, or domains in feature space, and are capable of a diverse range of spatiotemporal behavior on two-dimensional domains, including stationary and traveling bumps, breathers, traveling waves, stationary ring solutions, ring waves, target patterns, spiral waves, and other complex patterns [1–45]. A detailed review of stationary localized activity bumps and their existence, stability and applications on two-dimensional domains can be found in Ref. [35]. Inherent in the improvement of modeling equations for physical phenomena, such as spatiotemporal activity patterns in the brain [46–66] is a deeper understanding of the basic underlying spatiotemporal dynamics supported by these neural field equations and its relationship to model parameters and structure.

In addition to local field potential recordings and multielectrode arrays, the use of voltage-sensitive dyes and improved optical imaging techniques has been a primary approach to visualizing spatiotemporal activity in populations of neurons both in *in vitro* slice preparations of brain tissue under various pharmacological conditions [46–49,57,62,63] as well as *in vivo* experiments in both anesthetized [50,52,53,56,62,66–73] and awake behaving animals [51,71,72,74–77].

In *in vitro* cortical slice preparations, different spatiotemporal patterns of activity are observed under different pharmacological conditions including plane waves and outward propagating ring waves [46,48,49,51,60], collision and annihilation of plane waves [46], spiral waves [48,49], and evoked localized stationary activity in Refs. [47,61,63,76] which may be transient.

Spatiotemporal patterns in *in vivo* experimental preparations were also observed, including plane waves [53,54,59,62,64,68,73], periodic waves [76], circular waves [68,69,73], ring waves [68,73], spiral waves [68,72], and evoked localized stationary activity [50,62,64,66,67,70,78], often from sensory input, e.g., in somatosensory cortices S1 and S2 [67]. Additionally, evidence was found in Ref. [79] that was shown to be consistent with networks in prefrontal cortex supporting localized bumps of persistent neuronal activity during *in vivo* spatial working memory tasks in awake behaving animals during which the location of a stimulus is maintained in working memory as persistent activity.

*Contact author: sfolias@alaska.edu

In this paper we investigate the response in the activity of various networks of neuronal populations that support stationary localized bump and breather type solutions, both in the presence of a sustained, localized input inhomogeneity as well as in the input-free case. The localized input inhomogeneity could represent a diverse set of phenomena, including a sensory input to the layer, input from another brain region to the layer, a locally depolarized or hyperpolarized region within the layer, an external input due to an electrode or other external device, etc. We are interested in sustained responses of activity and whether they will be modulated by an oscillation.

The objective of this paper is three-fold and it builds upon and significantly extends our early work [15,20] in different ways, including a proper characterization of Hopf bifurcation in neural fields with O(2) symmetry. First, it compares results for linear stability and Hopf bifurcation of stationary bumps across a family of elementary neural fields with excitation, inhibition, and an adaptation or negative feedback gating variable on the two-dimensional domain $\mathbb{R}^2$ and includes a generalization and framework for N neural fields with M gating variables. Second, it comprehensively classifies the spatial structure of the eigenmodes and demonstrates its relation to the spatiotemporal structure of the time-periodic solutions emerging in a Hopf bifurcation and model parameters across all models. Third, it characterizes the conditions and results for a Hopf bifurcation with O(2) symmetry and its implication on the types of solutions that emerge in the Hopf bifurcation and their spatiotemporal symmetries and further verifies the solutions via numerical simulations across the family of neural fields.

We note that investigating the behavior of time-periodic solutions in numerical simulations of these neural fields can be confounded by secondary bifurcations, subcritical bifurcations, and coexistence of multiple stable attracting solutions as parameters are varied, particularly in the case of an input inhomogeneity that sustains activity far from the bifurcation point and in subcritical bifurcations. For clarity we are primarily focused on the emergent solutions in the vicinity of the critical point in a supercritical Hopf bifurcation of a stationary bump. We will leave the discussion of other types of periodic solutions for another treatment, although we briefly discuss some examples.

The family of elementary neural fields incorporates different forms of the fundamental types of excitatory and inhibitory synaptic inputs as well as an adaptation gating variable or negative feedback mechanism, which can model the process of spike-rate adaptation observed in neurons in cortex that decrease their firing rates after sustained firing. Adaptation serves as a concrete case to illustrate the incorporation of linear gating variables in the stability analysis for the generalization to more varied neural fields. It also compares two different dynamic mechanisms, nonlocal synaptic interactions and local negative feedback, that are capable of producing Hopf bifurcations of bumps. Interacting neural fields may represent different populations of neurons interacting nearby or across in a layer, between different layers, between different brain regions, etc.

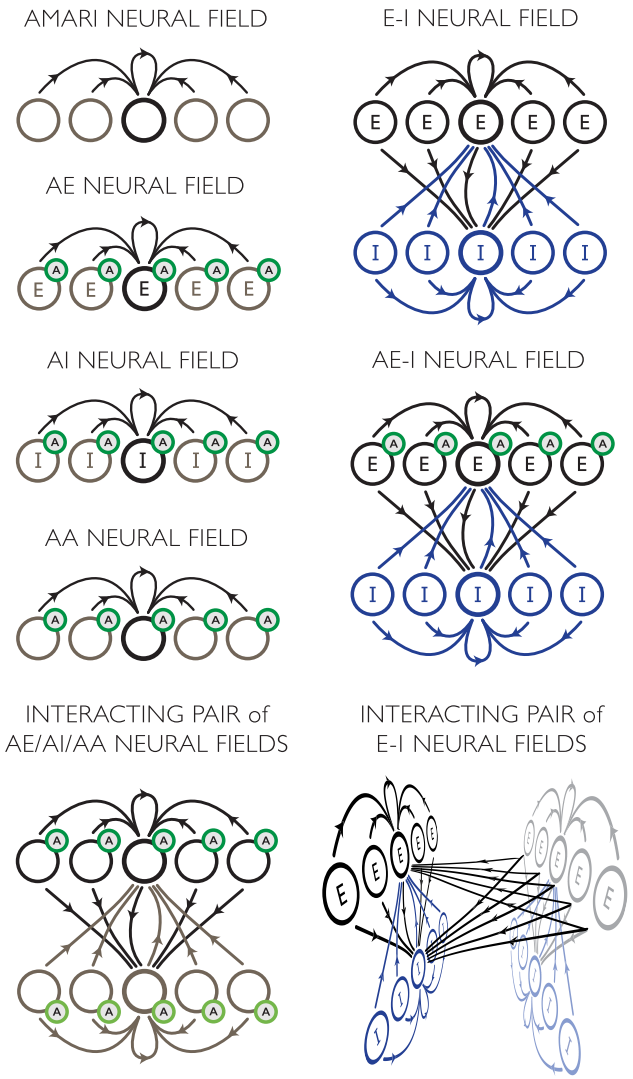

FIG. 1. Elementary neural fields on two-dimensional domains that support bumps, formed from a mixture of excitatory (E) and inhibitory (I) synaptic interactions with an additional adaptation (A) variable that modulates neuronal activity. AE and AI are single neural fields with either purely excitatory or inhibitory synaptic interaction, whereas AA is an Amari neural field (locally excitatory, laterally inhibitory) with an adaptation variable (A). E-I and AE-I are models with interacting excitatory and inhibitory neural fields, whereas in the AE-I model the excitatory neural field has an adaptation variable. Interacting pairs of neural fields refers to coupling together two of the same types of neural fields with choices about symmetry in parameters.

The paper is organized as follows. In Sec. II we outline a family of elementary neural fields depicted in Fig. 1 that are analyzed in the paper. In Sec. III we construct a general vectorized neural field model to analyze any configuration of N interacting neural fields with M gating variables and proceed to establish conditions for existence and stability of stationary bumps, including constructing eigenfunctions in the general case.

In Sec. IV we discuss an O(2) symmetric Hopf bifurcation in the case of radially symmetric synaptic weight functions and localized input inhomogeneity. This arises, in this case, for the eigenmodes associated with λ_n for $n \geqslant 1$ because the ordinary conditions for a Hopf bifurcation are not met due to the inherent symmetries of the synaptic connections and input inhomogeneity in the neural field equations.

In Sec. V we summarize formulas for two important integrals $W(r, a)$ and $\Omega_n(r, a)$ that the conditions for existence, linear stability and Hopf bifurcation of stationary bumps explicitly depend on in all models. We consider two classes of synaptic weight functions with different synaptic parameters in the form of (i) a *Gaussian* weight function and (ii) the *modified Bessel* weight function we introduced in Ref. [15] to approximate the exponential weight function $e^{-|r|}$ and simultaneously obtain closed-form expressions of $W(r, a)$ and $\Omega_n(r, a)$. These two classes of weight functions are used in concrete calculations, both for numerical simulations of the neural fields as well as numerical solutions of the analytical conditions for existence, stability and Hopf bifurcations of a stationary bump which are nonlinear.

In Sec. VI we apply the analysis in the vectorized case to the family of elementary neural field models with related symbols for direct comparison of the existence and stability results for stationary bumps in these models and discuss the spatiotemporal structure of the emergent time-periodic solutions that arise from a Hopf bifurcation with O(2) symmetry with respect to the different eigenmodes in the form of n-fold breathers with D_n dihedral symmetry or n-fold rotors with Z_n rotational symmetry. We also obtain conditions that determine which eigenmodes with different spatial structure destabilize in a Hopf bifurcation. In particular, in the interacting pairs of symmetric neural fields, we obtain conditions that determine whether an *in-phase* or *antiphase* periodic oscillation will occur in the two interacting neural field layers. We show it leads to families of synchronous breathers and rotors which could be *in-phase* or *antiphase*. Additionally in this section we show some examples of oscillatory solutions that occur far from the Hopf bifurcation point.

In Sec. VII we examine existence and stability of two examples of ring solutions in the E-I neural field, thereby extending our analysis to the case of ring solutions. Moreover, we use the linear stability analysis to demonstrate their destabilization in a Hopf bifurcation leads either to time-periodic n-fold ring breathers with D_n dihedral symmetry or rotors with Z_n rotational symmetry in numerical simulations of the neural field.

II. ELEMENTARY NEURAL FIELD MODELS

The neural field models studied in this paper are elementary models that involve different network topologies containing the two fundamental types of excitatory and inhibitory synaptic inputs generated either by separate populations of neurons or an effective mix in a simplified single population of neurons. We also incorporate a local linear negative feedback mechanism in the form of an adaptation gating variable, as a concrete example which models spike rate adaptation. The synaptic connectivity assumed in the analysis is based on short range connections found in regions of the cortex but can be generalized to other types of connectivity. Each neural field is capable of supporting stationary bumps that undergo Hopf bifurcation to time-oscillatory solutions. These fundamental building blocks can be used to build more complex neural field models supporting bumps.

In all models listed below, the synaptic weight functions $w_{jk}(r)$ are assumed to be distance-dependent, radially symmetric functions on $[0, \infty)$. We restrict to two classes of weight functions. We use a positive, monotonically decreasing weight function $w_{jk}(r)$ to represent synaptic interactions between neural fields that are purely excitatory or purely inhibitory between populations of neurons that are either excitatory or inhibitory [which is determined by a multiplicative sign (± 1)]. The second class is of a single synaptic weight function that abstractly represents the net excitatory or inhibitory input at different locations; in this scenario, we will assume a *Mexican hat* synaptic weight function, which is locally excitatory (at short distances) and laterally inhibitory (at greater distances). A Mexican hat weight function can be constructed by taking an appropriate difference of two positive weight functions $w(r) = w_e(r) - w_i(r)$ with different synaptic strengths $\bar{w}_j$ and space constants σ_j (see Sec. V). The firing rate nonlinearities are taken in the Heaviside limit $f(u) = H(u - \theta)$ with threshold θ.

For concrete calculations and numerical simulations, the synaptic weight functions $w_{jk}(r)$ are assumed to be either of the form of a Gaussian or a special modified Bessel weight function that we first introduced in Ref. [15] which permits calculation of all necessary expressions in closed form and approximates the exponential weight function $w(r) = e^{-r}$. The input inhomogeneity $I_j(r)$ is taken to be a Gaussian in concrete calculations. We list explicit calculations for these functions in Sec. V which are subsequently used in all in the neural field models.

The synaptic connectivity is translation invariant. Thus, in the input-free case $I_j(r) = 0$, the neural field is translation invariant. When $I_j = I_j(r)$ is a localized, radially symmetric Gaussian-like input inhomogeneity, centered at the origin, translation symmetry is broken.

Of the neural fields models listed, stability with respect to radial and angular perturbations and Hopf bifurcation of bumps were analyzed on two-dimensional domains in the AE/AA neural fields in Refs. [15,20]; however, the Hopf bifurcation to time-periodic solutions is clarified here.

We define the following symbol $w * f[u]$ for a nonlinear spatial convolution of a solution $u(\mathbf{r}, t)$ over $\mathbb{R}^2$, where

$$(w_{jk} * f[u])(\mathbf{r}, t) \;=\; \int_{\mathbb{R}^2} w_{jk}(\|\mathbf{r} - \mathbf{r}'\|) f(u(\mathbf{r}', t)) d^2\mathbf{r}',$$

represents the total synaptic input *from* neuronal population k at $\mathbf{r}' = (r', \theta')$ *to* neuronal population j at $\mathbf{r} = (r, \theta)$.

A. AE, AI, and AA neural field

$$\begin{aligned} \frac{\partial u}{\partial t} + u \;&=\; w * f[u] - \beta n + I(r), \\ \frac{1}{\alpha}\frac{\partial n}{\partial t} + n \;&=\; u, \end{aligned} \tag{1}$$

where $f(u) = H(u - \theta)$ and θ is a constant threshold. The AE *neural field* represents a layer of coupled excitatory (E) neurons ($u = u_e$) with positive coupling strength ($w(x) > 0$) subject to linear adaptation (A) in the form of the local negative feedback term $-\beta n$, where n is a gating-like variable governed by linear dynamics first introduced by Pinto and Ermentrout [3,7]. The AI *neural field* is a layer of coupled inhibitory (I) neurons ($u = u_i$) with negative synaptic coupling strength ($w(x) < 0$). The AA *neural field* is an *adapting* (A) form of the Amari (A) neural field where w is taken to be of Mexican hat form, which is an abstract simplified model, introduced by Amari [2], representing a mix of excitatory and inhibitory synaptic input to a layer of neurons ($u = u$). Though the Amari neural field is not specifically discussed here, Hopf bifurcations of stationary bumps do occur in the case of synaptic delays as analyzed in Ref. [36]. Moreover, other choices of w lead to different models [16].

B. E-I neural field

$$\begin{aligned}
\frac{\partial u_e}{\partial t} + u_e &= w_{ee} * f_e[u_e] - w_{ei} * f_i[u_i] + I_e(r),\\
\tau \frac{\partial u_i}{\partial t} + u_i &= w_{ie} * f_e[u_e] - w_{ii} * f_i[u_i] + I_i(r),
\end{aligned} \tag{2}$$

where we take $f_e(u) = H(u - \theta_e)$, $f_i(u) = H(u - \theta_i)$, and θ_e and θ_i are constant thresholds. The E-I *neural field* is a variant on the original Wilson-Cowan neural field [1]. We consider the formulation with all Heaviside nonlinearities introduced in Ref. [19]. An alternative formulation was considered in Ref. [8]. The synaptic weight functions w_{jk} are positive and synaptic currents are either excitatory or inhibitory.

C. AE-I neural field

$$\begin{aligned}
\frac{\partial u_e}{\partial t} + u_e &= w_{ee} * f_e[u_e] - w_{ei} * f_i[u_i] - \beta n_e + I_e,\\
\tau \frac{\partial u_i}{\partial t} + u_i &= w_{ie} * f_e[u_e] - w_{ii} * f_i[u_i] + I_i,\\
\frac{1}{\alpha}\frac{\partial n_e}{\partial t} + n_e &= u_e,
\end{aligned} \tag{3}$$

where we take $f_e(u) = H(u - \theta_e)$, $f_i(u) = H(u - \theta_i)$, where θ_e and θ_i are constant thresholds. The AE-I *neural field* is the two population E-I neural field where the E-population is subject to linear adaptation (A) introduced in Refs. [25,26].

D. Interacting AE/AA/AI neural fields

An interacting pair of Amari neural fields was introduced and studied in Refs. [32,33]. We introduce two forms interacting pairs of AA/AE/AI neural fields with *adaptation variables* n_1 and n_2: a *symmetric case* where the two neural fields are identical but are allowed to evolve independently and an *asymmetric case* where temporal dynamics are identical but synaptic weight functions, thresholds, and inputs differ.

Case I: Symmetric case

$$\begin{aligned}
\frac{\partial u_1}{\partial t} + u_1 &= w_{\rm loc} * f[u_1] + w_{\rm lay} * f[u_2] - \beta n_1 + I(r),\\
\frac{\partial u_2}{\partial t} + u_2 &= w_{\rm loc} * f[u_2] + w_{\rm lay} * f[u_1] - \beta n_2 + I(r),\\
\frac{1}{\alpha}\frac{\partial n_1}{\partial t} + n_1 &= u_1,\\
\frac{1}{\alpha}\frac{\partial n_2}{\partial t} + n_2 &= u_2,
\end{aligned} \tag{4}$$

where $f(u) = H(u - \theta)$ and θ is a constant threshold. Synaptic weight function $w_{\rm loc}$ represents the local connections within each population, whereas $w_{\rm lay}$ represents the interlayer synaptic connections from one population to the other. In this case, the two sets of synaptic weight functions are assumed to be identical for each population.

Case II: Asymmetric case

$$\begin{aligned}
\frac{\partial u_1}{\partial t} + u_1 &= w_{11}^{\rm loc} * f_1[u_1] + w_{12}^{\rm lay} * f_2[u_2] - \beta n_1 + I_1,\\
\frac{\partial u_2}{\partial t} + u_2 &= w_{22}^{\rm loc} * f_2[u_2] + w_{21}^{\rm lay} * f_1[u_1] - \beta n_2 + I_2,\\
\frac{1}{\alpha}\frac{\partial n_1}{\partial t} + n_1 &= u_1,\\
\frac{1}{\alpha}\frac{\partial n_2}{\partial t} + n_2 &= u_2,
\end{aligned} \tag{5}$$

where we take $f_1(u) = H(u - \theta_1)$ and $f_2(u) = H(u - \theta_2)$, and θ_1 and θ_2 are constant thresholds. In this case both the local and interlayer synaptic weight functions are allowed to be different but we still assume the weight functions are radially symmetric and translation invariant. The case of differing α_1, α_2 and β_1, β_2 is also treatable.

E. Interacting E-I neural fields

$$\begin{aligned}
\frac{\partial u_e}{\partial t} + u_e &= w_{ee}^{\rm loc} * f_e[u_e] - w_{ei}^{\rm loc} * f_i[u_i] + w_{ee}^{\rm lay} * f_e[v_e] + I_e,\\
\tau \frac{\partial u_i}{\partial t} + u_i &= w_{ie}^{\rm loc} * f_e[u_e] - w_{ii}^{\rm loc} * f_i[u_i] + w_{ie}^{\rm lay} * f_e[v_e] + I_i,\\
\frac{\partial v_e}{\partial t} + v_e &= w_{ee}^{\rm loc} * f_e[v_e] - w_{ei}^{\rm loc} * f_i[v_i] + w_{ee}^{\rm lay} * f_e[u_e] + I_e,\\
\tau \frac{\partial v_i}{\partial t} + v_i &= w_{ie}^{\rm loc} * f_e[v_e] - w_{ii}^{\rm loc} * f_i[v_i] + w_{ie}^{\rm lay} * f_e[u_e] + I_i,
\end{aligned} \tag{6}$$

where we take $f_e[u] = H(u - \theta_e)$, $f_i[u] = H(u - \theta_i)$, and θ_e and θ_i are constant thresholds. This neural field was introduced by Folias and Ermentrout in Refs. [32,33]. The interlayer connections between the E-I neural fields are excitatory (to model long-range connections in cortex) but inhibitory connections are similar. For simplicity the E-I neural fields are identical with symmetric connections.

III. ANALYSIS OF STATIONARY BUMPS

A. Notation

We define notation to move between vector and scalar notation for different steps of the analysis.

The notation $\mathbf{u} = [u_j]$ for $j = 1, ..., N$ will denote an N-dimensional vector whose jth element is the expression u_j which is a neural field or gating variable or related quantity. Subsequently, the notation $(\mathbf{u})_j$ is used to refer to jth element of any defined vector $\mathbf{u}$. The notation $\mathbf{M} = [\mathrm{M}_{jk}]$ for $j = 1, \ldots, M,\ k = 1, \ldots, N$ denotes an $(M\times N)$ matrix with element jk given by expression M_{jk}.

B. Structure of the neural fields on $\mathbb{R}^2$

We construct a vector formulation for a family of N neural fields on the two-dimensional domain $\mathbb{R}^2$ modulated by M linear gating variables, each coupled to only one neural field (each neural field may be coupled to more than one gating variable). We analyze the existence and stability of radially symmetric stationary bump solutions in the vector formulation along the lines we took in Ref. [15].

We consider two forms of a general neural field equation with N neural fields where the first is

$$\frac{\partial \mathbf{u}}{\partial t}(\mathbf{r}, t) = \mathbf{A}\mathbf{u}(\mathbf{r}, t) + \mathbf{W} * \mathbf{H}[\mathbf{u} - \theta] + \mathbf{I}(r), \tag{7}$$

with the vector $\mathbf{u} = [u_j(\mathbf{r}, t)]$ representing a vector of N neural fields $u_1,\ u_2, \ldots, u_N$ all defined on a universal spatial coordinate system on $\mathbb{R}^2$ and time t. We also consider a neural field equation with N neural fields u_j with M additional linear auxiliary or gating variables v_k

$$\begin{aligned}\frac{\partial \mathbf{u}}{\partial t}(\mathbf{r}, t) &= \mathbf{A}\mathbf{u}(\mathbf{r}, t) + \mathbf{B}\mathbf{v}(\mathbf{r}, t) + \mathbf{W} * \mathbf{H}[\mathbf{u} - \theta] + \mathbf{I}(r),\\ \frac{\partial \mathbf{v}}{\partial t}(\mathbf{r}, t) &= \mathbf{C}\mathbf{u}(\mathbf{r}, t) + \mathbf{D}\mathbf{v}(\mathbf{r}, t),\end{aligned} \tag{8}$$

where additionally $\mathbf{v} = [v_k(\mathbf{r}, t)]$ represents a vector of M auxiliary or gating variables $v_1,\ v_2, \ldots, v_M$. The input inhomogeneity $\mathbf{I}(r) = [I_j(r)]$ where $I_j(r)$ is radially symmetric about the origin, Gaussian-like, and taken to be excitatory (positive) or zero but could be inhibitory. For concreteness we take $I_j(r) = I_\circ^j e^{-(r/\sigma_j)^2}$. The case $\mathbf{I}(r) = \mathbf{0}$ represents the associated *input-free* neural field.

The synaptic kernel matrix $\mathbf{W}$ is defined in terms of distance-dependent synaptic coupling between $\mathbf{r} = (r, \theta)$ and $\mathbf{r}' = (r', \theta')$ as the $(N\times N)$ matrix function

$$\mathbf{W}(\|\mathbf{r} - \mathbf{r}'\|) = [w_{jk}(\|\mathbf{r} - \mathbf{r}'\|)]. \tag{9}$$

Synaptic weight functions w_{jk} mediate the synaptic inputs to *post-synaptic* population j at location $\mathbf{r}$ from the *pre-synaptic* population k at location $\mathbf{r}'$. In this section only, w_{jk} includes negative signs for pure inhibition.

The convolution is an integral over $\mathbb{R}^2$,

$$\mathbf{W} * \mathbf{H}[\mathbf{u} - \theta] = \int_{\mathbb{R}^2} \mathbf{W}(\|\mathbf{r} - \mathbf{r}'\|)\, \mathbf{H}[\mathbf{u}(\mathbf{r}', t) - \theta]\, d^2\mathbf{r}',$$

where

$$\mathbf{H}[\mathbf{u} - \theta] = \begin{bmatrix} H(u_1 - \theta_1) \\ H(u_2 - \theta_2) \\ \vdots \\ H(u_N - \theta_N) \end{bmatrix}$$

is a vector of Heaviside firing rate nonlinearities over the N populations u_j with thresholds θ_j (where $\theta = [\theta_j]$).

Different neural fields u_j are assumed to interact only through nonlinear synaptic interactions. Each gating variable is assumed to be coupled to one neural field only and evolve according to linear dynamics. These assumptions imply $\mathbf{A}$ is an $(N\times N)$ *diagonal* matrix, $\mathbf{D}$ is an $(M\times M)$ *diagonal* matrix, $\mathbf{B}$ is an $(N\times M)$ matrix, and $\mathbf{C}$ is an $(M\times N)$ matrix, which are assumed to be constant. Both $\mathbf{B}$ and $\mathbf{C}^{\mathrm{T}}$ have one nonzero entry in each column in the same location so nonzero entry jk of $\mathbf{B}$ aligns with nonzero entry kj in $\mathbf{C}$. This implies $\mathbf{B}\mathbf{D}^{-1}\mathbf{C}$ is *diagonal* whenever $\mathbf{D}$ is invertible since its nonzero elements occur when multiplying nonzero element jk of $\mathbf{B}$ with corresponding nonzero element kj of $\mathbf{C}$ which produces element jj on the diagonal, given that $\mathbf{D}^{-1}$ is diagonal. We shall assume $\mathbf{A}$, $\mathbf{D}$ and $(\mathbf{A} - \mathbf{B}\mathbf{D}^{-1}\mathbf{C})$ are invertible.

C. Stationary bump existence

We consider the existence of radially symmetric stationary bump solutions $\mathbf{u}(\mathbf{r}, t) = \mathbf{U}(r)$ of neural field equations (7) and (8) with spatial profile $\mathbf{U}(r) = [U_j(r)]$ that depends on radial coordinate r only. We assume profile $U_j(r)$ is a bounded function on $[0, \infty)$, satisfying the following threshold conditions for each neural field j

$$\begin{aligned} U_j(r) &> \theta_j, \quad r \in [0, a_j),\\ U_j(a_j) &= \theta_j, \quad r = a_j,\\ U_j(r) &< \theta_j, \quad r \in (a_j, \infty),\\ U_j(r) &\to 0, \quad \text{as } r \longrightarrow \infty. \end{aligned}$$

A stationary bump can be expressed as

$$\mathbf{u}(\mathbf{r}, t) = \mathbf{U}(r) = \mathbf{A}^{-1}(\boldsymbol{\mathcal{W}}(\mathbf{r}; \boldsymbol{a}) + \mathbf{I}(r)), \tag{10}$$

or, when gating variables are present, as follows below (where the diagonal matrix $\widetilde{\mathbf{A}} = \mathbf{A} - \mathbf{B}\mathbf{D}^{-1}\mathbf{C}$):

$$\begin{aligned}\mathbf{u}(\mathbf{r}, t) &= \mathbf{U}(r) \equiv \widetilde{\mathbf{A}}^{-1}(\boldsymbol{\mathcal{W}}(\mathbf{r}; \boldsymbol{a}) + \mathbf{I}(r)),\\ \mathbf{v}(\mathbf{r}, t) &= \mathbf{V}(r) \equiv -\mathbf{D}^{-1}\mathbf{C}\,\mathbf{U}(r; \boldsymbol{a}),\end{aligned} \tag{11}$$

and $\widetilde{\mathbf{A}}^{-1} = \mathrm{diag}(\widetilde{A}_{11}^{-1}, ..., \widetilde{A}_{NN}^{-1})$ which reduces to $\widetilde{\mathbf{A}} = \mathbf{A}$ in the case of no gating variables.

The convolution can be expressed as a vector function

$$\mathbf{W} * \mathbf{H}[\mathbf{u} - \theta] = \boldsymbol{\mathcal{W}}(r; \boldsymbol{a}) = [\,\mathcal{W}_j(r; \boldsymbol{a})]$$

with components $\mathcal{W}_j(r; \boldsymbol{a})$, where $\boldsymbol{a} = [a_j]$ given by

$$\mathcal{W}_j(r; \boldsymbol{a}) = \sum_{k=1}^{N} W_{jk}(r; a_k), \quad j = 1, ..., N,$$

where from our work in Ref. [15],

$$W_{jk}(r;a_k) = \int_{\mathbb{R}^2} w_{jk}(\|\mathbf{r}-\mathbf{r}'\|)H(U_k(r')-\theta_k)d^2\mathbf{r}'$$
$$= \int_0^{2\pi}\int_0^{a_k} w_{jk}(\|\mathbf{r}-\mathbf{r}'\|)r'dr'd\theta \quad (12)$$
$$= 2\pi a_k \int_0^{\infty} \breve{w}_{jk}(\rho)J_0(r\rho)J_1(a_k\rho)\,d\rho. \quad (13)$$

Functions W_{jk} are radially symmetric whenever w_{jk} and U_j are radially symmetric and, moreover, $W_{jk}(r;a_k)$ is monotonically decreasing in r whenever $w_{jk}(r)$ is monotonically decreasing in r as we have shown in Ref. [15]. The form in equation (13) is using the Fourier integral representation expressed in terms of $\breve{w}$, which is the *Hankel transform of order 0* of synaptic weight function $w(r)$,

$$w(r) = \int_0^{\infty} \breve{w}_{jk}(\rho)J_0(r\rho)\rho\,d\rho. \quad (14)$$

$J_n(r)$ is the Bessel function of the first kind of order n. The Hankel transform is the two-dimensional Fourier transform for radially symmetric functions on $\mathbb{R}^2$[15,80]. Expressions for $W_{jk}(r;a_k)$ in the case of specific forms of the synaptic weight functions are given in Sec. V.

The stationary bump solution is $\mathbf{U}=[U_j]$ where the jth component can be expressed as

$$U_j(r) = \frac{1}{\widetilde{A}_{jj}}\left(\sum_{k=1}^{N} W_{jk}(r;a_k) + I_j(r)\right). \quad (15)$$

D. Stationary bump stability

We now analyze the evolution of small time-dependent perturbations of the stationary bump solution through linear stability analysis. The behavior of the system near and beyond the Hopf bifurcation is then studied in numerical simulations as in one dimension.

Equation (8) is linearized about the stationary solution $(\mathbf{U},\mathbf{V})$ by introducing the time-dependent perturbations

$$\mathbf{u}(\mathbf{r},t) = \mathbf{U}(r) + \widetilde{\boldsymbol{\varphi}}(\mathbf{r},t),$$
$$\mathbf{v}(\mathbf{r},t) = \mathbf{V}(r) + \widetilde{\boldsymbol{\psi}}(\mathbf{r},t),$$

and expanding to first order in $\widetilde{\boldsymbol{\varphi}}, \widetilde{\boldsymbol{\psi}}$ which leads to the linear system of integrodifferential equations

$$\frac{\partial}{\partial t}\widetilde{\boldsymbol{\varphi}} = \mathbf{A}\widetilde{\boldsymbol{\varphi}} + \mathbf{B}\widetilde{\boldsymbol{\psi}} + \mathbf{N}\widetilde{\boldsymbol{\varphi}},$$
$$\frac{\partial}{\partial t}\widetilde{\boldsymbol{\psi}} = \mathbf{C}\widetilde{\boldsymbol{\varphi}} + \mathbf{D}\widetilde{\boldsymbol{\psi}}. \quad (16)$$

where $\mathbf{N}$ is a nonlocal compact linear operator given by

$$\mathbf{N}\boldsymbol{\varphi} = \mathbf{W} * [\boldsymbol{\delta}(\mathbf{U}-\boldsymbol{\theta})\boldsymbol{\varphi}]$$
$$= \int_{\mathbb{R}^2} \mathbf{W}(||\mathbf{r}-\mathbf{r}'||)\,\boldsymbol{\delta}(\mathbf{U}(r)-\boldsymbol{\theta})\,\boldsymbol{\varphi}(\mathbf{r}')\,d^2\mathbf{r}'.$$

$\mathbf{W}$ is the matrix of synaptic weight functions in Eq. (9) and $\boldsymbol{\delta}(\mathbf{U}-\boldsymbol{\theta})\boldsymbol{\varphi}$ is the vector of δ functions over the N neural fields φ_j with thresholds θ_j and bump profiles $U_j(r)$,

$$\boldsymbol{\delta}(\mathbf{U}-\boldsymbol{\theta})\boldsymbol{\varphi} = \begin{bmatrix} \delta(U_1-\theta_1)\,\varphi_1 \\ \delta(U_2-\theta_2)\,\varphi_2 \\ \vdots \\ \delta(U_N-\theta_N)\,\varphi_N \end{bmatrix}.$$

Setting $\widetilde{\boldsymbol{\varphi}}(\mathbf{r},t) = \boldsymbol{\varphi}(\mathbf{r})e^{\lambda t}$ and $\widetilde{\boldsymbol{\psi}}(\mathbf{r},t) = \boldsymbol{\psi}(\mathbf{r})e^{\lambda t}$ in Eq. (16) results in the *spectral problem*

$$\lambda\,\boldsymbol{\varphi} = \mathbf{A}\boldsymbol{\varphi} + \mathbf{B}\boldsymbol{\psi} + \mathbf{N}\boldsymbol{\varphi},$$
$$\lambda\,\boldsymbol{\psi} = \mathbf{C}\boldsymbol{\varphi} + \mathbf{D}\boldsymbol{\psi}. \quad (17)$$

When matrix $(\lambda\mathbf{I}-\mathbf{D})$ is invertible, $\boldsymbol{\psi} = (\lambda\mathbf{I}-\mathbf{D})^{-1}\mathbf{C}\boldsymbol{\varphi}$ is determined uniquely by $\boldsymbol{\varphi}$ thereby reducing (17) to the *reduced spectral problem*

$$(\mathbf{L}(\lambda)+\mathbf{N})\boldsymbol{\varphi} = \lambda\,\boldsymbol{\varphi}, \quad (18)$$

where matrix operator $\mathbf{L}(\lambda) = \mathbf{A} + \mathbf{B}(\lambda\mathbf{I}-\mathbf{D})^{-1}\mathbf{C}$ depends on the spectral parameter λ. When linear gating variables are not present, $\mathbf{L}(\lambda)$ reduces to $\mathbf{L}(\lambda)=\mathbf{A}$.

For $\mathbf{A},\mathbf{B},\mathbf{C},\mathbf{D}$ satisfying the assumptions in Sec. III B, it follows that $\mathbf{L}(\lambda)$ is *diagonal* whenever $(\lambda\mathbf{I}-\mathbf{D})$ is invertible. To reference the elements of $\mathbf{L}(\lambda)$ we define

$$\mathbf{L}(\lambda) = \mathsf{diag}(\ell_{11}(\lambda), \ell_{22}(\lambda), \ldots \ell_{NN}(\lambda)).$$

We view operator $\mathbf{N}$ acting on the vector function $\boldsymbol{\varphi}(\mathbf{r})$ as a matrix of nonlocal integral operators $\mathcal{N}_{jk}$

$$\mathbf{N} = [\mathcal{N}_{jk}],$$

each acting on its scalar component $\varphi_k(x)$ according to

$$\mathcal{N}_{jk}\,\varphi_k(r,\theta) = w_{jk} * [H'(U_k-\theta_k)\,\varphi_k]$$
$$= \int_{\mathbb{R}^2} w_{jk}(\|\mathbf{r}-\mathbf{r}'\|)\,\delta(U_k(r')-\theta_k)\,\varphi_k(\mathbf{r}')\,d^2\mathbf{r}'$$
$$= \int_0^{2\pi}\int_0^{\infty} w_{jk}\left(\sqrt{r^2+(r')^2-2rr'\cos(\theta-\theta')}\right)$$
$$\times\ \delta(U_k(r')-\theta_k)\varphi_k(r',\theta')\,r'\,dr'd\theta'$$
$$= \frac{1}{|U_k'(a_k)|}\,a_k\int_0^{2\pi} w_{jk}\left(\sqrt{r^2+a_k^2-2ra_k\cos(\phi)}\right)$$
$$\times\ \varphi_k(a_k,\theta-\phi)\,d\phi$$

where $|U_k'(a_k)|$ is calculated from Eq. (15) by differentiating

$$U_j'(r) = \frac{1}{\widetilde{A}_{jj}}\left(\sum_{k=1}^{N}\frac{\partial W_{jk}}{\partial r}(r;a_k) + I_j'(r)\right),$$

and expressions for $\frac{\partial W_{jk}}{\partial r}(r;a_k)$ are calculated in Sec. V.

1. Essential spectrum

The essential spectra of $(\mathbf{L}+\mathbf{N})$ and $\mathbf{L}$ are the same, since $\mathbf{N}$ is a compact operator and $\mathbf{L}+\mathbf{N}$ is a compact perturbation of $\mathbf{L}$, and comprise the finite set of values

$$\sigma_{\mathsf{ess}} = \{\lambda_i^{\mathsf{ess}}\}_{i=1}^{Q},$$

where σ_{ess} is the set of all solutions to the equation

$$\prod_{j=1}^{N}(\ell_{jj}(\lambda)-\lambda)=0,$$

where $\ell_{jj}(\lambda)$ are the diagonal elements of $\mathbf{L}(\lambda)$ and $\ell_{jj}(\lambda)=A_{jj}$ when no gating variables are present. $(\mathbf{L}(\lambda)-\lambda\mathbf{I})$ has an infinite-dimensional kernel formed from functions with arbitrary spatial dependence satisfying $\mathbf{N}\boldsymbol{\varphi}=\mathbf{0}$. Since $(\mathbf{L}+\mathbf{N})$ and $\mathbf{L}$ are closed operators and these λ_i^{ess} are isolated points of the spectrum with infinite geometric multiplicity, it follows that they belong to the essential spectrum of $\mathbf{L}$ and $(\mathbf{L}+\mathbf{N})$ [81]. The essential spectrum lies in the open left-half complex plane whenever $\Re\mathrm{e}\{\lambda_i^{\text{ess}}\}<0$ for all $i=1,\ldots,Q$. In this case, spectral stability of the stationary bump is determined by eigenvalues λ in the point spectrum which occur when spectral problem (18) has nontrivial solutions $\boldsymbol{\varphi}(r,\theta)$.

2. Point spectrum

Solutions to the system of linear integral equations (18) (with continuity conditions at $\theta=\pm\pi$) are of the form

$$\boldsymbol{\varphi}_n(r,\theta)=\boldsymbol{\Phi}_n(r)e^{in\theta}\quad n\in\mathbb{Z}$$

where the radial component $\boldsymbol{\Phi}_n=[\Phi_n^j(r)]$ satisfies the following nonlocal equation for $j=1,\ldots,N$

$$(\lambda-\ell_{jj}(\lambda))\Phi_n^j(r) \;=\; \sum_{k=1}^{N}\frac{\Omega_n^{jk}(r;a_k)}{|U_k'(a_k)|}\Phi_n^k(a_k), \tag{19}$$

where

$$\Omega_n^{jk}(r;a_k)=a_k\int_0^{2\pi}w_{jk}\Big(\sqrt{r^2+a_k^2-2ra_k\cos(\phi)}\,\Big)\cos(n\phi)\,d\phi.$$

$\Phi_n^j(r)$ is determined by its value $\Phi_n^j(a_j)$ at $r=a_j$ and the N unknown values $\Phi_n^j(a_j)$ are determined by requiring (19) to hold at the restriction to $r=a_j$ for $j=1,\ldots,N$ resulting in the following compatibility condition:

$$(\lambda-\ell_{jj}(\lambda))\Phi_n^j(a_j) \;=\; \sum_{k=1}^{N}\mathcal{M}_n^{jk}(a_j;a_k)\Phi_n^k(a_k) \tag{20}$$

where $\mathcal{M}_n^{jk}(a_j;a_k)=\Omega_n^{jk}(a_j;a_k)/|U_k'(a_k)|$. Compatibility condition (20) can be expressed compactly as

$$(\lambda\mathbf{I}-\mathbf{L}(\lambda))\boldsymbol{\phi}_n=\mathbf{M}_n\boldsymbol{\phi}_n, \tag{21}$$

where matrix $\mathbf{M}_n=[\mathcal{M}_n^{jk}(a_j;a_k)]$ and $\boldsymbol{\phi}_n=[\Phi_n^j(a_j)]$ is the vector of special nonlocal values.

Rewriting *compatibility condition* (21) as

$$(\lambda\mathbf{I}-\mathbf{L}(\lambda)-\mathbf{M}_n)\boldsymbol{\phi}_n=\mathbf{0}, \tag{22}$$

nontrivial solutions $\boldsymbol{\phi}_n$ exist for the set $\lambda\notin\sigma_{\text{ess}}$ whenever $\det(\lambda\mathbf{I}-\mathbf{L}(\lambda)-\mathbf{M}_n)=0$ giving rise to eigenvalues λ_n and eigenfunctions $\boldsymbol{\varphi}_n(r,\theta)$ of the nth eigenmode on the set of λ where $(\lambda\mathbf{I}-\mathbf{L}(\lambda))$ is invertible. Note that the set where $(\lambda\mathbf{I}-\mathbf{L}(\lambda))$ is not invertible coincides with the essential spectrum σ_{ess}. Consequently, an *Evans function* $\mathcal{E}_n(\lambda)$ for the nth *eigenmode* of the linearization about the stationary bump $\mathbf{u}(x)$ is given by

$$\mathcal{E}_n(\lambda)=\det(\lambda\mathbf{I}-\mathbf{L}(\lambda)-\mathbf{M}_n). \tag{23}$$

Eigenvalues λ_n of the nonlocal operator $(\mathbf{L}(\lambda)+\mathbf{N})$ are given by the zero sets of $\mathcal{E}_n(\lambda)$ for $n=0,1,2,\ldots$.

3. Construction of the eigenspaces

Since the eigenfunctions are vector functions of the form $(\boldsymbol{\varphi}(r,\theta),\boldsymbol{\psi}(r,\theta))$ where $\boldsymbol{\psi}(r,\theta)=(\lambda\mathbf{I}-\mathbf{D})^{-1}\mathbf{C}\boldsymbol{\varphi}(r,\theta)$, we concentrate on component $\boldsymbol{\varphi}(r,\theta)$. Eigenvalues λ_0 associated with the $n=0$ mode correspond to one-dimensional eigenspaces spanned by radially symmetric eigenfunction

$$\boldsymbol{\varphi}_0(r,\theta) \;=\; \boldsymbol{\mathcal{C}}_0(\lambda)\,\boldsymbol{\mathcal{M}}_0(r)\,\boldsymbol{\phi}_0,$$

and each eigenvalue λ_n has a two-dimensional eigenspace for $n\geqslant 1$ spanned by two linearly independent functions

$$\boldsymbol{\varphi}_n^1(r,\theta) \;=\; \hat{\boldsymbol{\varphi}}_n(r)\,e^{in\theta},\qquad \hat{\boldsymbol{\varphi}}_n(r) \;=\; \boldsymbol{\mathcal{C}}_n(\lambda)\,\boldsymbol{\mathcal{M}}_n(r)\,\boldsymbol{\phi}_n,$$
$$\boldsymbol{\varphi}_n^2(r,\theta) \;=\; \hat{\boldsymbol{\varphi}}_n(r)\,e^{-in\theta},$$

where $\boldsymbol{\mathcal{C}}_n(\lambda)=(\lambda_n\mathbf{I}-\mathbf{L}(\lambda_n))^{-1}=\mathrm{diag}((\lambda_n-\ell_{jj}(\lambda_n))^{-1})$ is a constant diagonal matrix and

$$\boldsymbol{\mathcal{M}}_n(r) \;=\; \big[\,\mathcal{M}_n^{jk}(r;a_k)\,\big],\;\; \mathcal{M}_n^{jk}(r;a_k)=\frac{\Omega_n^{jk}(r;a_k)}{|U_k'(a_k)|}, \tag{24}$$

and $j,k=1,\ldots,N$. The jth component of the vector expression $\hat{\boldsymbol{\varphi}}_n(r)$ for $j=1,\ldots,N$ can be written as

$$(\hat{\boldsymbol{\varphi}}_n(r))_j=\frac{1}{(\lambda_n-\ell_{jj}(\lambda_n))}\sum_{k=1}^{N}\left(\frac{\Phi_n^k(a_k)}{|U_k'(a_k)|}\right)\Omega_n^{jk}(r;a_k)$$
$$\overset{\text{OR}}{=}\;\Phi_n^j(a_j)\frac{\sum_{k=1}^{N}\mathcal{M}_n^{jk}(r;a_k)\Phi_n^k(a_k)}{\sum_{k=1}^{N}\mathcal{M}_n^{jk}(a_j;a_k)\Phi_n^k(a_k)}, \tag{25}$$

where the last expression comes from using Eq. (20). The profiles $\Omega_n^{jk}(r;a_k)e^{in\theta}$ determine the spatial structure of the eigenmode. (See Sec. V for explicit calculations.)

The spatial eigenspaces for eigenmodes $n\geqslant 1$ generically are two-dimensional and spanned by two linearly independent eigenfunctions $\boldsymbol{\varphi}_n^1(r,\theta)$ and $\boldsymbol{\varphi}_n^2(r,\theta)$ as stated above, which could be written in real form with $\cos(n\theta)$ and $\sin(n\theta)$. This multiplicity arises from the rotational symmetry and continuity or boundary conditions in the angular coordinate θ. We discuss the implication of this multiplicity on the Hopf bifurcation of stationary solutions in Sec. IV.

IV. HOPF BIFURCATION WITH O(2) SYMMETRY

Due to the symmetry in our 2D neural field equations, care must be taken in the stability analysis to determine how the spatial eigenmodes (indexed by n) destabilize via Hopf bifurcation and lead to the spatial structure of time-periodic solutions that emerge in the bifurcation. The issue is that the usual conditions for a Hopf bifurcation are not met for spatial eigenmodes $n\geqslant 1$ because two pairs of eigenvalues are simultaneously becoming critical whenever one of these modes destabilizes in a Hopf bifurcation. This can be seen from the fact that for $n\geqslant 1$ the spatial eigenspaces are two-dimensional (spanned by two eigenfunctions, containing $e^{\pm in\theta}$ or $\cos(n\theta)$ and $\sin(n\theta)$) due to rotational symmetry and continuity conditions in θ. Consequently, the geometric and algebraic multiplicity of the critical eigenvalues are both

2. In contrast, in the $n = 0$ case, each eigenspace is one-dimensional.

When the eigenvalue multiplicity is greater than 1 due to symmetry present in our equations, the equivariant Hopf theorem from equivariant bifurcation theory and group theory [82] provides a rigorous Hopf bifurcation theorem as well as a characterization of the number of bifurcating solutions and their spatiotemporal symmetries, based upon the relevant symmetry groups.

Although breathers occur in neural field models without input inhomogeneities, most of the cases we have considered are in the presence of a localized input inhomogeneity $I(r) = I(\|\mathbf{r}\|)$ which breaks translation symmetry in the Euclidean group. So we consider O(2) (the orthogonal group of rotations and reflections of the plane that keep the origin fixed) as the relevant symmetry group for our neural fields since the localized input inhomogeneity is radially symmetric and centered at the origin. Consequently, $\mathrm{O}(2) \times \mathbf{S}^1$ is the relevant spatiotemporal symmetry group for the symmetric Hopf bifurcation, where $\mathbf{S}^1$ is the circle group of temporal phase shifts acting on the space of 2π-periodic functions.

The spatiotemporal structure of the periodic solutions emerging in a Hopf bifurcation with O(2) symmetry, according to the equivariant Hopf theorem [82], are determined by the specific conjugacy classes of isotropy subgroups in $\mathrm{O}(2) \times \mathbf{S}^1$ that have two-dimensional fixed point subspaces which, using the standard action, are $\widetilde{\mathbf{SO}}(2)$ and $Z_2(\kappa) \oplus Z_2^c(\pi, \pi)$. Isotropy subgroups of periodic solutions are formed from the spatial and spatiotemporal symmetries that leave the periodic solution invariant. The equivariant Hopf theorem indicates that two branches of periodic solutions simultaneously bifurcate from the equilibrium, one corresponding to each of these isotropy subgroups which we describe below. However, the equations for the spatial eigenmodes (indexed by n) have an additional rotational symmetry Z_n (reflected by $e^{in\theta}$ in the eigenfunctions), consequently Z_n is added to the isotropy subgroups for the nth eigenmode via a nonstandard action wherein Z_n acts trivially, imposing additional symmetry on the bifurcating solution branches from higher spatial eigenmodes $n \geqslant 2$ as discussed below.

The two branches of periodic solutions bifurcating from the equilibrium may appear on either side of the Hopf bifurcation point where an equilibrium loses stability. When one or both branches of solutions are subcritical (meaning that, when varying a parameter, they appear on the side of the bifurcation point where the eigenvalues have negative real part, prior to the destabilization of the equilibrium) then both periodic solutions are unstable. For one of the periodic solutions to be stable, both branches of solutions must be supercritical (meaning that, when varying a parameter, they appear on the side of the bifurcation point where the eigenvalues have positive real part and the equilibrium is unstable) in which case, depending on higher-order terms, one of the two branches of solutions is orbitally asymptotically stable (meaning that solutions in a neighborhood of the periodic solution approach the orbit of the periodic solution as $t \longrightarrow \infty$).

All periodic solutions have a spatiotemporal symmetry that spatial rotation by angle π is equivalent to a temporal phase shift of π (or half a period of time), i.e., $R_\pi\, \mathbf{u}(t) = \mathbf{u}(t + \pi)$ since spatiotemporal symmetry $(\pi, \pi) \in \mathrm{O}(2) \times \mathbf{S}^1$ acts trivially. However the isotropy subgroups with two-dimensional fixed point subspaces dictate the remaining symmetries of the different branches of periodic solutions which we now describe.

Periodic solutions with isotropy subgroup $\widetilde{\mathbf{SO}}(2) = \{(\theta, \theta) \in \mathbf{SO}(2) \times \mathbf{S}^1\}$ satisfy a *spatiotemporal* symmetry property that spatial rotation by angle θ has the same effect as temporal phase shift by θ (or $\theta/2\pi$ of a period), i.e., $R_\theta\, \mathbf{u}(t) = \mathbf{u}(t + \theta)$, giving rise to time-periodic solutions that take the form of *rotating waves* about a point. Moreover, the bifurcating rotating waves associated with the nth *eigenmode* have an additional cyclic group symmetry Z_n (invariance under spatial rotations by $2\pi/n$).

Periodic solutions with isotropy $Z_2(\kappa) \oplus Z_2^c(\pi, \pi) = \langle \kappa, (\pi, \pi) \rangle$ however, satisfy a *spatial* symmetry property of invariance under a reflection κ across an axis through the origin at all instants of time ($\kappa\, \mathbf{u}(t) = \mathbf{u}(t)$), which gives rise to time-periodic solutions in the form of *standing waves*. The standing waves associated with the nth *eigenmode* have an additional dihedral group symmetry D_n (invariance under rotations and reflections that preserve an n-gon) due to the combination of the reflection κ with the additional rotational symmetry Z_n of the nth eigenmode ($D_n = \langle \kappa, Z_n \rangle$).

We shall assume an equivariant Hopf theorem holds and proceed to verify our neural field equations are equivariant with respect to the symmetry group O(2) on $\mathbb{R}^2$.

$\gamma \in \mathrm{O}(2)$ is a symmetry of $\frac{\partial \mathbf{u}}{\partial t} = F(\mathbf{u}, \mu)$ if $\gamma\mathbf{u}$ is a solution whenever $\mathbf{u}$ is a solution. This holds whenever γ satisfies the commutivity relation

$$\gamma \cdot F(\mathbf{u}, \mu) = F(\gamma \cdot \mathbf{u}, \mu).$$

Such functions F are said to be *equivariant* with respect to the symmetry. If F and $\frac{\partial \mathbf{u}}{\partial t} = F(\mathbf{u}, \mu)$ satisfy this for all $\gamma \in \mathrm{O}(2)$, then they are said to be *equivariant* with respect to O(2). To show that our neural field equations satisfy this, the action of O(2) on $\mathbb{R}^2$ is given by

$$\theta \cdot \mathbf{r} = R_\theta \mathbf{r},$$
$$\kappa \cdot \mathbf{r} = \kappa \mathbf{r},$$

where $\mathbf{r} = (x, y)$, $\kappa\mathbf{r} = (x, -y)$, and R_θ is the usual rotation matrix by angle θ. The group action on a function $f(\mathbf{r})$ is given by

$$\gamma \cdot f(\mathbf{r}) = f(\gamma^{-1} \cdot \mathbf{r}),$$

and the group action on the weight function $w(\mathbf{r}, \mathbf{r}')$ is

$$\gamma \cdot w(\mathbf{r}, \mathbf{r}') = w(\gamma^{-1} \cdot \mathbf{r}, \gamma^{-1} \cdot \mathbf{r}').$$

For both $\gamma = \theta$ (rotations about the origin by angle θ) and $\gamma = \kappa$ (reflections), our weight functions of the form $w(\mathbf{r}, \mathbf{r}') = \hat{w}(\|\mathbf{r} - \mathbf{r}'\|)$ naturally satisfy

$$w(\gamma^{-1} \cdot \mathbf{r}, \gamma^{-1} \cdot \mathbf{r}') = w(\mathbf{r}, \mathbf{r}'),$$

TABLE I. The existence and stability results depend on the functions $W(r;a)$ and $\Omega_n(r,a)$ listed in Eq. (26) which are calculated explicitly for a family of Gaussian and modified Bessel synaptic weight functions. $I_n(x)$ and $K_n(x)$ denote the *modified Bessel functions of the first and second kind of order n* and $L_n(x)$ denotes the *Laguerre polynomial of order n*. All expressions are finite sums of elementary/special functions and exact, except for the Gaussian where $W(r;a)$ is expressed as an infinite series.

	Explicit calculations for integrals in the analysis of stationary bumps on $\mathbb{R}^2$	
	$w(r) = \frac{\bar{w}}{\pi\sigma^2} e^{-(\frac{r}{\sigma})^2}$	$w(r) = \frac{2\bar{w}}{3\pi\sigma^2}[K_0(\frac{r}{\sigma}) - K_0(\frac{2r}{\sigma})]$
$W(r;a)$	$\bar{w} e^{-\frac{r^2}{\sigma^2}} \sum_{n=0}^{\infty} \frac{(-1)^n}{(n+1)!} (\frac{a}{\sigma})^{2n+2} L_n(\frac{r^2}{\sigma^2})$	$\begin{cases} \bar{w}\, \frac{4a}{3\sigma}\left[K_0(\frac{r}{\sigma})I_1(\frac{a}{\sigma}) - \frac{1}{2}K_0(\frac{2r}{\sigma})I_1(\frac{2a}{\sigma})\right] & r \geqslant a \\ \bar{w}\left(1 - \frac{4a}{3\sigma}[K_1(\frac{a}{\sigma})I_0(\frac{r}{\sigma}) - \frac{1}{2}K_1(\frac{2a}{\sigma})I_0(\frac{2r}{\sigma})]\right) & r < a \end{cases}$
$W(a;a)$	$\frac{\bar{w}}{2}\left[1 - e^{-\frac{2a^2}{\sigma^2}} I_0(\frac{2a^2}{\sigma^2})\right]$	$\bar{w}\, \frac{4a}{3\sigma}\left[K_0(\frac{a}{\sigma})I_1(\frac{a}{\sigma}) - \frac{1}{2}K_0(\frac{2a}{\sigma})I_1(\frac{2a}{\sigma})\right]$
$\frac{\partial W}{\partial r}(r;a)$	$-\bar{w}\, \frac{2a}{\sigma^2} e^{-\frac{r^2+a^2}{\sigma^2}} I_1(\frac{2ar}{\sigma^2})$	$\begin{cases} -\bar{w}\, \frac{4a}{3\sigma^2}\left[K_1(\frac{r}{\sigma})I_1(\frac{a}{\sigma}) - K_1(\frac{2r}{\sigma})I_1(\frac{2a}{\sigma})\right] & r \geqslant a \\ -\bar{w}\, \frac{4a}{3\sigma^2}\left[K_1(\frac{a}{\sigma})I_1(\frac{r}{\sigma}) - K_1(\frac{2a}{\sigma})I_1(\frac{2r}{\sigma})\right] & r < a \end{cases}$
$\frac{\partial W}{\partial r}(a;a)$	$-\bar{w}\, \frac{2a}{\sigma^2} e^{-\frac{2a^2}{\sigma^2}} I_1(\frac{2a^2}{\sigma^2})$	$-\bar{w}\, \frac{4a}{3\sigma^2}\left[K_1(\frac{a}{\sigma})I_1(\frac{a}{\sigma}) - K_1(\frac{2a}{\sigma})I_1(\frac{2a}{\sigma})\right]$
$\Omega_n(r;a)$	$\bar{w}\, \frac{2a}{\sigma^2} e^{-\frac{r^2+a^2}{\sigma^2}} I_n(\frac{2ar}{\sigma^2})$	$\begin{cases} \bar{w}\, \frac{4a}{3\sigma^2}\left[K_n(\frac{r}{\sigma})I_n(\frac{a}{\sigma}) - K_n(\frac{2r}{\sigma})I_n(\frac{2a}{\sigma})\right] & r \geqslant a \\ \bar{w}\, \frac{4a}{3\sigma^2}\left[K_n(\frac{a}{\sigma})I_n(\frac{r}{\sigma}) - K_n(\frac{2a}{\sigma})I_n(\frac{2r}{\sigma})\right] & r < a \end{cases}$
$\Omega_n(a;a)$	$\bar{w}\, \frac{2a}{\sigma^2} e^{-\frac{2a^2}{\sigma^2}} I_n(\frac{2a^2}{\sigma^2})$	$\bar{w}\, \frac{4a}{3\sigma^2}\left[K_n(\frac{a}{\sigma})I_n(\frac{a}{\sigma}) - K_n(\frac{2a}{\sigma})I_n(\frac{2a}{\sigma})\right]$

since (omitting the dot $\cdot$ henceforth)

$$w(\gamma^{-1}\mathbf{r}, \gamma^{-1}\mathbf{r}') = \hat{w}(\|\gamma^{-1}\mathbf{r} - \gamma^{-1}\mathbf{r}'\|) = \hat{w}(\|\gamma^{-1}(\mathbf{r} - \mathbf{r}')\|) = \hat{w}(\|\mathbf{r} - \mathbf{r}\|) = w(\mathbf{r}, \mathbf{r}').$$

This means $w(\gamma^{-1}\mathbf{r}, \mathbf{r}') = w(\mathbf{r}, \gamma\mathbf{r}')$, since

$$\hat{w}(\|\gamma^{-1}\mathbf{r} - \mathbf{r}'\|) = \hat{w}(\|\gamma(\gamma^{-1}\mathbf{r} - \mathbf{r}')\|) = \hat{w}(\|\mathbf{r} - \gamma\mathbf{r}'\|).$$

Consider the simplest form of the neural field equations considered here (which can be generalized to other cases):

$$\frac{\partial u}{\partial t}(\mathbf{r}, t) + u(\mathbf{r}, t) = \int_{\mathbb{R}^2} w(\mathbf{r}, \mathbf{r}') f(u(\mathbf{r}', t)) d^2\mathbf{r}' + I(\|\mathbf{r}\|).$$

The group action on a solution is $\gamma u(\mathbf{r}, t) = u(\gamma^{-1}\mathbf{r}, t)$ and the group action on the neural field equation is

$$\begin{aligned} &\frac{\partial u}{\partial t}(\gamma^{-1}\mathbf{r}, t) + u(\gamma^{-1}\mathbf{r}, t) \\ &\quad = \int_{\mathbb{R}^2} w(\gamma^{-1}\mathbf{r}, \mathbf{r}') f(u(\mathbf{r}', t)) d^2\mathbf{r}' + I(\|\gamma^{-1}\mathbf{r}\|) \\ &\quad = \int_{\mathbb{R}^2} w(\mathbf{r}, \gamma\mathbf{r}') f(u(\mathbf{r}', t)) d^2\mathbf{r}' + I(\|\mathbf{r}\|) \\ &\quad = \int_{\mathbb{R}^2} w(\mathbf{r}, \hat{\mathbf{r}}) f(u(\gamma^{-1}\hat{\mathbf{r}}, t)) d^2\hat{\mathbf{r}} + I(\|\mathbf{r}\|), \end{aligned}$$

where $\hat{\mathbf{r}} = \gamma\mathbf{r}'$ and $d^2\mathbf{r}' = d^2(\gamma^{-1}\hat{\mathbf{r}}) = |\pm 1| d^2\hat{\mathbf{r}}$. Since $\gamma u(\mathbf{r}, t) = u(\gamma^{-1}\mathbf{r}, t)$, this shows that $\gamma u(\mathbf{r}, t)$ is a solution whenever $u(\mathbf{r}, t)$ is a solution to our neural field equation. It also shows that $\gamma F(u) = F(\gamma u)$ where $F(u) = w * f(u)$ is the nonlinear synaptic convolution term. Therefore both the synaptic convolutions $w * f(u)$ and the neural field equation are equivariant with respect to O(2). Moreover, since all of our synaptic convolution terms and neural field equations are of the same general form, it can be shown that all are equivariant with respect to O(2).

V. EXPLICIT INTEGRAL CALCULATIONS FOR SYNAPTIC WEIGHT FUNCTIONS

We briefly (i) summarize the definitions of two important symbols and (ii) provide exact expressions for these quantities in Table I for two specific weight functions.

A. Formulas

Closed form expressions for the integral formulas for functions $W_{jk}(r;a_k)$ and $\Omega_n^{jk}(r;a_k)$ in the analysis that need to be calculated explicitly are summarized here. Note that in Table I the weight function indices jk have been dropped for simplicity:

$$\begin{aligned} W_{jk}(r;a_k) &= \int_0^{2\pi} \int_0^{a_k} w_{jk}(\|\mathbf{r} - \mathbf{r}'\|) r' dr' d\theta \\ &= 2\pi a_k \int_0^{\infty} \breve{w}_{jk}(\rho) J_0(r\rho) J_1(a_k\rho)\, d\rho, \\ \Omega_n^{jk}(r;a_k) &= a_k \int_0^{2\pi} w_{jk}(\sqrt{r^2 + a_k{}^2 - 2ra_k \cos(\phi)}) \cos(n\phi)\, d\phi \\ &= 2\pi a_k \int_0^{\infty} \breve{w}_{jk}(\rho) J_n(r\rho) J_n(a_k\rho)\, d\rho, \end{aligned} \tag{26}$$

where $\breve{w}_{jk}(\rho)$ represents the *Hankel transform of order 0* of synaptic weight function $w_{jk}(r)$.

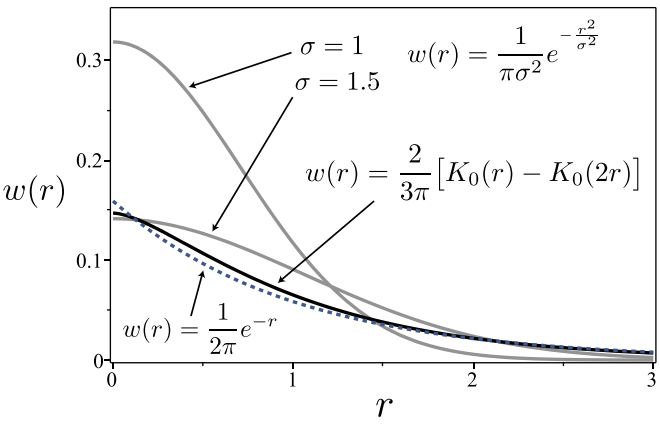

FIG. 2. Plots of the *Gaussian* (solid gray), *exponential* (dashed gray), and *modified Bessel* (solid black) synaptic weight functions with $\overline{w} = 1$ and $\sigma = 1$ except where indicated. All weight functions are normalized so their integral over $\mathbb{R}^2$ equals 1. Due to the rapid decay of the Gaussian, two plots of the Gaussian are shown, with case $\sigma = 1.5$ included as it is similar to the other weight functions near $r = 0$. The modified Bessel weight function well approximates the exponential case and permits exact calculation of the necessary expressions for the existence and stability calculations [15].

B. Positive weight functions

For explicit calculations and numerical simulations the following two forms of synaptic weight functions were used:

$$\text{Gaussian:} \quad w(r) = \frac{\overline{w}}{\pi\sigma^2} e^{-(\frac{r}{\sigma})^2}$$

$$\text{Modified Bessel:} \quad w(r) = \frac{2}{3\pi}\frac{\overline{w}}{\sigma^2}\left[K_0\left(\frac{r}{\sigma}\right) - K_0\left(\frac{2r}{\sigma}\right)\right].$$

We introduced this modified Bessel weight function [15] since the difference of Bessel functions well approximated the exponential weight function $\frac{1}{2\pi}e^{-r}$ and permitted the exact calculation of important integrals in closed form. K_0 denotes the modified Bessel function of the first kind of order 0. Some properties of the modified Bessel weight function are listed below for clarity

$$\lim_{r\to 0^+} w(r) = \frac{\overline{w}}{\sigma^2}\frac{1}{2\pi}\cdot\frac{4}{3}\ln(2) \approx \frac{\overline{w}}{\sigma^2}\frac{1}{2\pi}0.924$$

$$\lim_{r\to 0^+} w'(r) = 0$$

$$w(r) \sim \frac{\overline{w}}{3\sqrt{\pi}\sigma^{\frac{3}{2}}}\left(\frac{\sqrt{2}e^{-\frac{r}{\sigma}} - e^{-\frac{2r}{\sigma}}}{\sqrt{r}}\right), \quad \text{for large } r.$$

A comparison between the modified Bessel, Gaussian, and exponential weight functions is illustrated in Fig. 2.

C. Mexican hat weight function

A *Mexican hat* weight function can be formulated by adding two positive weight functions with different parameters and negating one of them to generate a mixture of excitation and inhibition in the following form:

$$w_M(r) = w(r\,;\,\bar{w}_e, \sigma_e) - w(r\,;\,\bar{w}_i, \sigma_i), \tag{27}$$

where $\bar{w}_e$, $\bar{w}_i$, σ_e, and σ_i are positive constants associated with excitation and inhibition that are chosen so that the function is locally positive (near $r = 0$) and laterally negative (for large enough r) [2]. This would be switched for an *inverted Mexican hat* which is locally negative near $r = 0$ and laterally positive for large enough r. Such functions provide an abstraction allowing a single neural field layer to generate both excitation and inhibition.

VI. EXISTENCE AND STABILITY OF BUMPS IN ELEMENTARY NEURAL FIELDS ON $\mathbb{R}^2$

The stationary bump solutions and stability analysis for each of the neural fields explored in this section can be expressed in terms of integrals listed in Sec. V with different neural fields denoted by various subscripts. In all cases a stationary bump solution is a bounded solution $U_j(r)$ on $[0, \infty)$ in which there is a bump in each neural field variable indexed by j satisfying the threshold condition $U_j(a_j) = \theta_j$ with $U_j(r) > \theta_j$ for $r \in [0, a_j)$ and $U_j(r) < \theta_j$ otherwise.

Linear stability of the stationary bump is analyzed and the essential spectrum σ_{ess} is determined to be negative in all of the models and thereby not a cause of instability. Stability of the stationary bump is consequently determined by the eigenvalues in the point spectrum and eigenvalues and eigenfunctions are constructed. A stationary bump is *linearly stable* if all eigenvalues have negative real part except the generic 0-eigenvalue associated with translation invariance of stationary solutions in neural fields with translation symmetry. This holds for the neural fields in this section in the absence of input inhomogeneities and the translation mode cannot destabilize in a Hopf bifurcation in this case except possibly in the AE-I neural field. When input inhomogeneities are introduced, translation symmetry is broken and the translation eigenmode ($n = 1$) has a pair of nonzero eigenvalues that can become complex and lead to a Hopf bifurcation.

A. AE, AI, and AA neural fields

A stationary bump solution to neural field equation (1) with radius a is $(u(\mathbf{r}, t), n(\mathbf{r}, t)) = (U(r), N(r))$ where

$$(1 + \beta)U(r) = W(r; a) + I(r),$$
$$N(r) = U(r),$$

and the radius a is determined by the threshold condition

$$W(a; a) + I(a) = \theta(1 + \beta)$$

provided $U(r)$ obeys the threshold behavior on $(0, \infty)$.

Time-dependent perturbations $(\widetilde{\varphi}(\mathbf{r}, t), \widetilde{\psi}(\mathbf{r}, t))$ of the stationary bump $(U(r), N(r))$ evolve according to

$$\frac{\partial\widetilde{\varphi}}{\partial t} + \widetilde{\varphi} = \mathcal{N}\widetilde{\varphi} - \beta\widetilde{\psi},$$
$$\frac{1}{\alpha}\frac{\partial\widetilde{\psi}}{\partial t} + \widetilde{\psi} = \widetilde{\varphi}. \tag{28}$$

Setting $(\widetilde{\varphi}, \widetilde{\psi}) = \boldsymbol{\varphi}(\mathbf{r})e^{\lambda t}$ results in the spectral problem for λ and $\boldsymbol{\varphi}(\mathbf{r}) = (\varphi(\mathbf{r}), \psi(\mathbf{r}))$,

$$-\varphi + \mathcal{N}\varphi - \beta\psi = \lambda\varphi$$
$$\alpha\varphi - \alpha\psi = \lambda\psi. \tag{29}$$

Setting $\varphi(r,\theta)=\hat{\varphi}(r)e^{in\theta}$ and $\psi(r,\theta)=(\frac{\alpha}{\lambda+\alpha})\varphi(r,\theta)$ the compatibility equation determining the eigenvalues and special nonlocal values of the eigenfunctions at the threshold point $r=a$ is given by

$$(\mathcal{M}_n(a;a)-1)\hat{\varphi}(a)=\left(\lambda+\frac{\alpha\beta}{\lambda+\alpha}\right)\hat{\varphi}(a), \tag{30}$$

where $\mathcal{M}_n(a;a)=\Omega_n(a;a)/|U'(a)|$. Compatibility equation (30) can be rewritten as

$$(\mathcal{M}_n(a;a)-\mu(\lambda))\boldsymbol{\phi}_n=0, \tag{31}$$

where $\mu(\lambda)=1+\lambda+\frac{\alpha\beta}{\lambda+\alpha}$ and $\boldsymbol{\phi}_n=\hat{\varphi}(a)$. Nontrivial solutions to Eq. (31) exist only when

$$\mu(\lambda)=\mathcal{M}_n(a;a),$$

then solving for λ we obtain

$$\lambda_n=-\Gamma\pm\sqrt{\Gamma^2-\Delta^2},\quad \Gamma=\tfrac{1}{2}(1+\alpha-\mu_n),$$
$$\mu_n=\mathcal{M}_n(a;a),\quad \Delta=\alpha(1+\beta-\mu_n).$$

The special nonlocal value can take on any fixed value (generating a family of eigenfunctions); for simplicity we set $\boldsymbol{\phi}_n=\hat{\varphi}(a)=1$. Spatial eigenfunctions $\boldsymbol{\varphi}_n(r,\theta)$ for each eigenvalue λ in the nth eigenmode are given by

$$\boldsymbol{\varphi}_n^1(r,\theta)=\hat{\boldsymbol{\varphi}}_n(r)e^{in\theta},$$
$$\boldsymbol{\varphi}_n^2(r,\theta)=\hat{\boldsymbol{\varphi}}_n(r)e^{-in\theta},$$

where

$$\hat{\boldsymbol{\varphi}}_n(r)=\begin{pmatrix}\hat{\varphi}_n(r)\\ \hat{\psi}_n(r)\end{pmatrix}=\begin{pmatrix}1\\ \frac{\alpha}{\lambda_n+\alpha}\end{pmatrix}\mathcal{M}_n(r;a),$$

where $\mathcal{M}_n(r;a)=\Omega_n(r;a)/|U'(a)|$. Note that, in a real basis for the eigenspace, the eigenfunctions for the neural field variable φ in this case could be expressed as

$$\varphi_n^1(r,\theta)=\mathcal{M}_n(r;a)\cos(n\theta),$$
$$\varphi_n^2(r,\theta)=\mathcal{M}_n(r;a)\sin(n\theta).$$

At a Hopf bifurcation point the Hopf frequency is

$$\omega_H=\mathsf{Im}\{\lambda_n\}=\sqrt{\alpha(\beta-\alpha)}.$$

B. E-I neural field

A stationary bump solution to neural field equation (2) is $(u_e(\mathbf{r},t),u_i(\mathbf{r},t))=(U_e(r),U_i(r))$, where

$$U_e(r)=W_{ee}(r;a_e)-W_{ei}(r;a_i)+I_e(r),$$
$$U_i(r)=W_{ie}(r;a_e)-W_{ii}(r;a_i)+I_i(r),$$

and the radii a_e and a_i satisfy the threshold conditions

$$W_{ee}(a_e;a_e)-W_{ei}(a_e;a_i)+I_e(a_e)=\theta_e$$
$$W_{ie}(a_i;a_e)-W_{ii}(a_i;a_i)+I_i(a_i)=\theta_i$$

provided the threshold behavior is obeyed on $(0,\infty)$.

Time-dependent perturbations $(\widetilde{\varphi}_e(\mathbf{r},t),\widetilde{\varphi}_i(\mathbf{r},t))$ of the stationary bump $(U_e(r),U_i(r))$ evolve according to

$$\frac{\partial\widetilde{\varphi}_e}{\partial t}+\widetilde{\varphi}_e=\mathcal{N}_{ee}\widetilde{\varphi}_e-\mathcal{N}_{ei}\widetilde{\varphi}_i,$$
$$\tau\frac{\partial\widetilde{\varphi}_i}{\partial t}+\widetilde{\varphi}_i=\mathcal{N}_{ie}\widetilde{\varphi}_e-\mathcal{N}_{ii}\widetilde{\varphi}_i. \tag{32}$$

Setting $(\widetilde{\varphi}_e,\widetilde{\varphi}_i)=\boldsymbol{\varphi}(\mathbf{r})e^{\lambda t}$ leads to the spectral problem for λ and $\boldsymbol{\varphi}(\mathbf{r})=(\varphi_e(\mathbf{r}),\varphi_i(\mathbf{r}))$:

$$-\varphi_e+\mathcal{N}_{ee}\varphi_e-\mathcal{N}_{ei}\varphi_i=\lambda\varphi_e,$$
$$-\frac{1}{\tau}\varphi_i+\frac{1}{\tau}\mathcal{N}_{ie}\varphi_e-\frac{1}{\tau}\mathcal{N}_{ii}\varphi_i=\lambda\varphi_i. \tag{33}$$

Setting $\varphi_e(r,\theta)=\hat{\varphi}_e(r)e^{in\theta}$ and $\varphi_i(r,\theta)=\hat{\varphi}_i(r)e^{in\theta}$ the compatibility equation determining both the eigenvalues and special nonlocal values of the eigenfunctions for the nth eigenmode at threshold points $r=a_e,a_i$ is

$$\left(\mathbf{M}_n^{\mathrm{EI}}-\mathbf{I}_{\mathrm{EI}}\right)\boldsymbol{\phi}_n=\lambda\,\boldsymbol{\phi}_n, \tag{34}$$

where $\mathbf{I}_{\mathrm{EI}}=\mathsf{diag}\,(1,\tau^{-1})$

$$\mathbf{M}_n^{\mathrm{EI}}=\begin{bmatrix}\mathcal{M}_n^{ee}(a_e;a_e) & -\mathcal{M}_n^{ei}(a_e;a_i)\\ \frac{1}{\tau}\mathcal{M}_n^{ie}(a_i;a_e) & -\frac{1}{\tau}\mathcal{M}_n^{ii}(a_i;a_i)\end{bmatrix},\quad \boldsymbol{\phi}_n=\begin{pmatrix}\hat{\varphi}_e(a_e)\\ \hat{\varphi}_i(a_i)\end{pmatrix},$$

and $\mathcal{M}_n^{jk}(a_j;a_k)=\Omega_n^{jk}(a_j;a_k)/|U_k'(a_k)|$. Condition (34) can be rewritten as

$$\left(\mathbf{M}_n^{\mathrm{EI}}-\mathbf{D}(\lambda)\right)\boldsymbol{\phi}_n=0, \tag{35}$$

where $\mathbf{D}(\lambda)=\mathsf{diag}\,(1+\lambda,\frac{1}{\tau}+\lambda)$. Equation (35) has nontrivial solutions when $\mathsf{det}(\mathbf{M}_n^{\mathrm{EI}}-\mathbf{D}(\lambda))=0$ Solving for the eigenvalues λ we obtain

$$\lambda_n=\left[\frac{\mathcal{M}_n^{ee}-1}{2}-\frac{\mathcal{M}_n^{ii}+1}{2\tau}\right]\pm\sqrt{\left[\frac{\mathcal{M}_n^{ee}-1}{2}+\frac{\mathcal{M}_n^{ii}+1}{2\tau}\right]^2-\frac{\mathcal{M}_n^{ei}\mathcal{M}_n^{ie}}{\tau}},$$

where $\mathcal{M}_n^{jk}=\mathcal{M}_n^{jk}(a_j,a_k)$. The corresponding vector of special nonlocal values may be expressed in the form $\boldsymbol{\phi}_n=(\hat{\varphi}_e(a_e),\hat{\varphi}_i(a_i))=(1,\nu_n)$, where

$$\nu_n=\frac{\lambda_n+1-\mathcal{M}_n^{ee}(a_e;a_e)}{-\mathcal{M}_n^{ei}(a_e;a_i)}=\frac{\left[\frac{\mathcal{M}_n^{ee}-1}{2}+\frac{\mathcal{M}_n^{ii}+1}{2\tau}\right]\pm\sqrt{\left[\frac{\mathcal{M}_n^{ee}-1}{2}+\frac{\mathcal{M}_n^{ii}+1}{2\tau}\right]^2-\frac{\mathcal{M}_n^{ei}\mathcal{M}_n^{ie}}{\tau}}}{-\mathcal{M}_n^{ei}}$$

and $\mathcal{M}_n^{jk}=\mathcal{M}_n^{jk}(a_j;a_k)$. Spatial eigenfunctions $\boldsymbol{\varphi}_n(r,\theta)$ for an eigenvalue λ in the nth eigenmode are

$$\boldsymbol{\varphi}_n^1(r,\theta)=\hat{\boldsymbol{\varphi}}_n(r)e^{in\theta},$$
$$\boldsymbol{\varphi}_n^2(r,\theta)=\hat{\boldsymbol{\varphi}}_n(r)e^{-in\theta},$$

where

$$\hat{\boldsymbol{\varphi}}_n(r)=\begin{pmatrix}\hat{\varphi}_e^n\\ \hat{\varphi}_i^n\end{pmatrix}=\begin{pmatrix}\frac{1}{\lambda+1}\left[\mathcal{M}_n^{ee}(r;a_e)-\nu_n\mathcal{M}_n^{ei}(r;a_i)\right]\\ \frac{1}{\tau\lambda+1}\left[\mathcal{M}_n^{ie}(r;a_e)-\nu_n\mathcal{M}_n^{ii}(r;a_i)\right]\end{pmatrix}.$$

At a Hopf bifurcation point the Hopf frequency is

$$\omega_H=\mathsf{Im}\{\lambda_n\}=\sqrt{\frac{-(\mathcal{M}_n^{ee}-1)(\mathcal{M}_n^{ii}+1)+\mathcal{M}_n^{ei}\mathcal{M}_n^{ie}}{\tau}},$$

where $(\mathcal{M}_n^{ee}-1)=(\mathcal{M}_n^{ii}+1)/\tau$.

See Figs. 3 and 4 for examples of expanding-contracting breathers and rotors exhibiting n-fold symmetry in the E-I

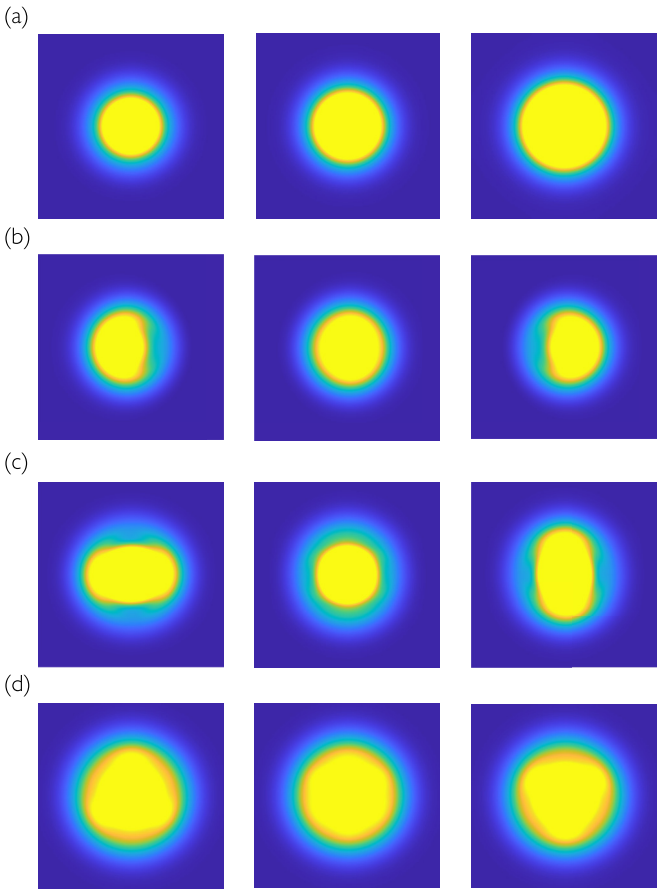

FIG. 3. n-fold *breathers* or expanding-contracting *stationary waves* in the E-I neural field model as a result of the destabilization of a stationary bump solution via Hopf bifurcation with respect to eigenmodes with different spatial structure: (a) destabilization of the $n = 0$ mode leading to a radially symmetric breather; (b) destabilization of the $n = 1$ mode leading to a onefold breather with D_1 dihedral symmetry; (c) destabilization of the $n = 2$ mode leading to a onefold breather with D_2 dihedral symmetry; (d) destabilization of the $n = 3$ mode leading to a threefold breather with D_3 dihedral symmetry. Lighter/warmer colors (orange and yellow) indicate values above threshold θ_e and darker/cooler colors indicate subthreshold values.

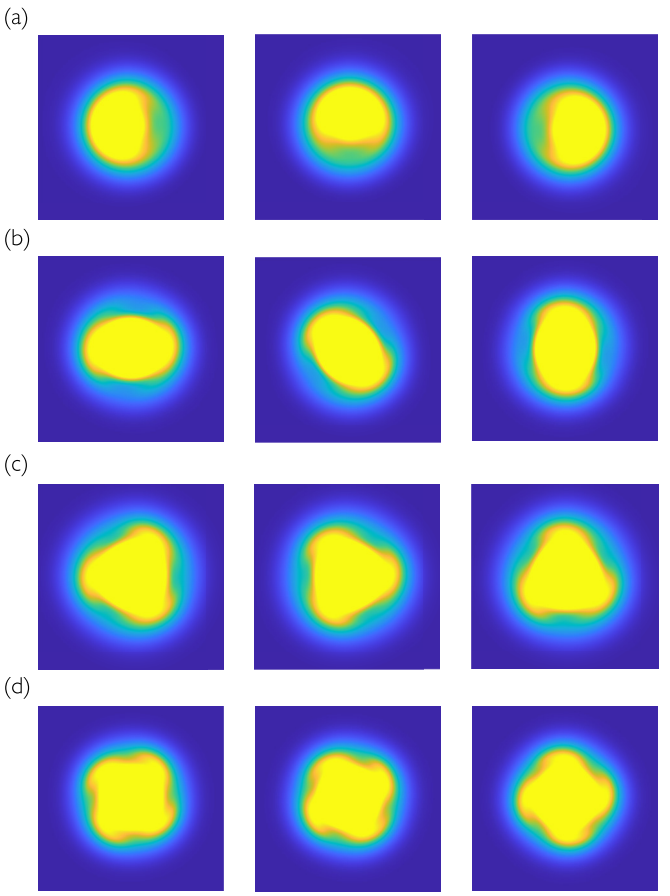

FIG. 4. n-fold *rotors* or *rotating waves* in the E-I neural field model at different points in time t resulting from the destabilization of a stationary bump via Hopf bifurcation with respect to eigenmodes with different spatial structure: (a) destabilization of the $n = 1$ mode leading to a onefold rotor with Z_1 rotational symmetry; (b) destabilization of the $n = 2$ mode leading to a twofold rotor with Z_2 rotational symmetry; (c) destabilization of the $n = 3$ mode leading to a threefold rotor with Z_3 rotational symmetry; (d) destabilization of the $n = 4$ mode leading to a fourfold rotor with Z_4 rotational symmetry. Lighter/warmer colors (orange and yellow) indicate values above threshold θ_e and darker/cooler colors indicate subthreshold values.

neural field. Figure 5 depicts a complicated oscillatory solution well beyond a Hopf bifurcation point where the $n = 3$ eigenmode destabilizes in the E-I neural field.

C. AE-I neural field

A stationary bump solution to neural field equation (3) is $(u_e(\mathbf{r}, t), u_i(\mathbf{r}, t), n_e(\mathbf{r}, t)) = (U_e(r), U_i(r), N_e(r))$, where

$$\begin{aligned}(1+\beta)U_e(r) &= W_{ee}(r;a_e) - W_{ei}(r;a_i) + I_e(r),\\ U_i(r) &= W_{ie}(r;a_e) - W_{ii}(r;a_i) + I_i(r),\\ N_e(r) &= U_e(r),\end{aligned}$$

where the radii a_e and a_i satisfy the threshold conditions

$$\begin{aligned}W_{ee}(a_e;a_e) - W_{ei}(a_e;a_i) + I_e(a_e) &= \theta_e(1+\beta)\\ W_{ie}(a_i;a_e) - W_{ii}(a_i;a_i) + I_i(a_i) &= \theta_i\end{aligned}$$

provided the threshold behavior is obeyed on $(0, \infty)$.

Time-dependent perturbations $(\widetilde{\varphi}_e, \widetilde{\varphi}_i, \widetilde{\psi}_e)(\mathbf{r}, t)$ of a stationary bump $(U_e(r), U_i(r), N_e(r))$ evolve according to

$$\begin{aligned}\frac{\partial\widetilde{\varphi}_e}{\partial t} + \widetilde{\varphi}_e &= \mathcal{N}_{ee}\,\widetilde{\varphi}_e - \mathcal{N}_{ei}\,\widetilde{\varphi}_i - \beta\widetilde{\psi}_e,\\ \tau\frac{\partial\widetilde{\varphi}_i}{\partial t} + \widetilde{\varphi}_i &= \mathcal{N}_{ie}\,\widetilde{\varphi}_e - \mathcal{N}_{ii}\,\widetilde{\varphi}_i,\\ \frac{1}{\alpha}\frac{\partial\widetilde{\psi}_e}{\partial t} + \widetilde{\psi}_e &= \widetilde{\varphi}_e.\end{aligned} \tag{36}$$

Setting $(\widetilde{\varphi}_e, \widetilde{\varphi}_i, \widetilde{\psi}_e) = \boldsymbol{\varphi}(\mathbf{r})e^{\lambda t}$ results in the spectral problem for λ and $\boldsymbol{\varphi}(\mathbf{r}) = (\varphi_e(\mathbf{r}), \varphi_i(\mathbf{r}), \psi_e(\mathbf{r}))$:

$$\begin{aligned}-\varphi_e + \mathcal{N}_{ee}\,\varphi_e - \mathcal{N}_{ei}\,\varphi_i - \beta\psi_e &= \lambda\varphi_e,\\ -\frac{1}{\tau}\varphi_i + \frac{1}{\tau}\mathcal{N}_{ie}\,\varphi_e - \frac{1}{\tau}\mathcal{N}_{ii}\,\varphi_i &= \lambda\varphi_i,\\ \alpha\varphi_e - \alpha\psi_e &= \lambda\psi_e.\end{aligned} \tag{37}$$

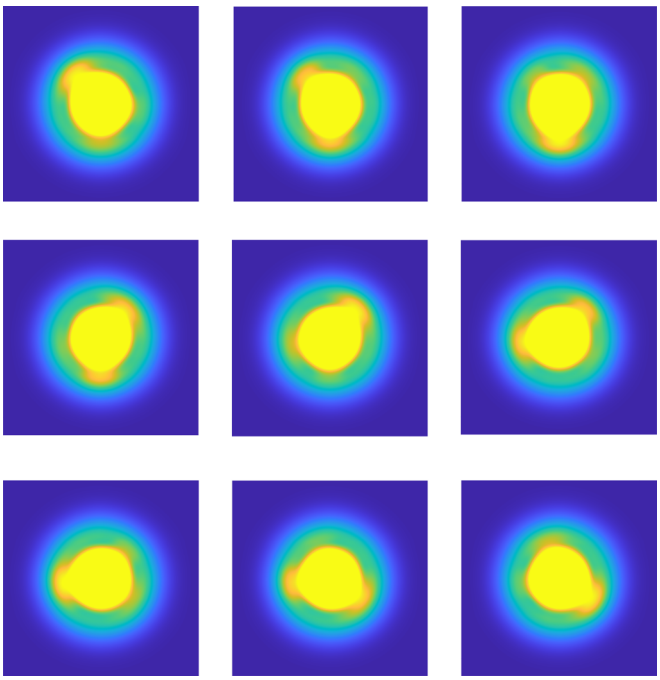

FIG. 5. Examples of a complicated oscillatory solution in the E-I neural field in a parameter region where multiple eigenmodes have complex eigenvalues with negative real part and both the $n = 3$ and $n = 2$ (and other modes) destabilize at different locations. A small lobe on the boundary of the activity bump emerges and then retracts at different points during the oscillatory behavior that appears to have a three-prong structure. The lobes continually emerge at different locations, and long-term plotting of the orbit projected onto the phase plane for different spatial locations (not shown) appears to show a complicated attractor in the projection.

Setting

$$\varphi_e(r,\theta) = \hat{\varphi}_e(r)e^{in\theta},$$
$$\varphi_i(r,\theta) = \hat{\varphi}_i(r)e^{in\theta},$$
$$\psi_e(r,\theta) = \left(\frac{\alpha}{\lambda+\alpha}\right)\varphi_e(r,\theta),$$

the compatibility equation determining both the eigenvalues and special nonlocal values of the eigenfunctions of the nth eigenmode at threshold points a_e and a_i is

$$\left(\mathbf{M}_n^{\mathrm{EI}} - \mathbf{I}_{\mathrm{EI}}\right)\boldsymbol{\phi}_n = \begin{bmatrix} \lambda + \frac{\alpha\beta}{\lambda+\alpha} & 0 \\ 0 & \lambda \end{bmatrix}\boldsymbol{\phi}_n, \tag{38}$$

where $\mathbf{I}_{\mathrm{EI}} = \mathsf{diag}\,(1, \tau^{-1})$ and

$$\mathbf{M}_n^{\mathrm{EI}} = \begin{bmatrix} \mathcal{M}_n^{ee}(a_e;a_e) & -\mathcal{M}_n^{ei}(a_e;a_i) \\ \frac{1}{\tau}\mathcal{M}_n^{ie}(a_i;a_e) & -\frac{1}{\tau}\mathcal{M}_n^{ii}(a_i;a_i) \end{bmatrix}, \boldsymbol{\phi}_n = \begin{pmatrix} \hat{\varphi}_e(a_e) \\ \hat{\varphi}_i(a_i) \end{pmatrix}$$

and $\mathcal{M}_n^{jk}(a_j;a_k) = \Omega_n^{jk}(a_j;a_k)/|U_k'(a_k)|$. Compatibility condition (38) can be rewritten as

$$\left(\mathbf{M}_n^{\mathrm{EI}} - \mathbf{D}(\lambda)\right)\boldsymbol{\phi}_n = 0, \tag{39}$$

where $\mathbf{D}(\lambda) = \mathsf{diag}\,(1 + \lambda + \frac{\alpha\beta}{\lambda+\alpha}, \frac{1}{\tau} + \lambda)$, which has nontrivial solutions when λ satisfies $\mathsf{det}(\mathbf{M}_n^{\mathrm{EI}} - \mathbf{D}(\lambda)) = 0$.

Eigenvalues thereby satisfy the following cubic equation:

$$\tau\lambda^3 + \Gamma_n\lambda^2 + \Delta_n\lambda + \mathrm{E}_n = 0,$$

where the coefficients are given by

$$\begin{aligned}
\Gamma_n &= \tau\left[\alpha + 1 - \mathcal{M}_n^{ee}(a_e;a_e)\right] + \left[1 + \mathcal{M}_n^{ii}(a_i;a_i)\right], \\
\Delta_n &= \left[\alpha + 1 - \mathcal{M}_n^{ee}(a_e;a_e)\right]\left[\tau\alpha + 1 + \mathcal{M}_n^{ii}(a_i;a_i)\right] \\
&\quad + \mathcal{M}_n^{ei}(a_e;a_i)\mathcal{M}_n^{ie}(a_i;a_e) + \tau\alpha(\beta - \alpha), \\
\mathrm{E}_n &= \alpha\left[\beta + 1 - \mathcal{M}_n^{ee}(a_e;a_e)\right]\left[1 + \mathcal{M}_n^{ii}(a_i;a_i)\right] \\
&\quad + \alpha\left[\mathcal{M}_n^{ei}(a_e;a_i)\mathcal{M}_n^{ie}(a_i;a_e)\right].
\end{aligned}$$

Solving Eq. (38) for the vector of special nonlocal values in the form $\boldsymbol{\phi}_n = (\hat{\varphi}_e(a_e), \hat{\varphi}_i(a_i)) = (1, \nu_n)$ we obtain

$$\nu_n = \frac{\lambda_n + \frac{\alpha}{\lambda_n+\alpha} + 1 - \mathcal{M}_n^{ee}(a_e;a_e)}{-\mathcal{M}_n^{ei}(a_e;a_i)}.$$

The spatial eigenfunctions $\boldsymbol{\varphi}_n(r,\theta)$ for an eigenvalue λ the nth eigenmode are given by

$$\boldsymbol{\varphi}_n^1(r,\theta) = \hat{\boldsymbol{\varphi}}_n(r)e^{in\theta}, \quad \boldsymbol{\varphi}_n^2(r,\theta) = \hat{\boldsymbol{\varphi}}_n(r)e^{-in\theta},$$

where $\mu(\lambda) = \lambda + 1 + \frac{\alpha\beta}{\lambda+\alpha}$ and

$$\hat{\boldsymbol{\varphi}}_n(r) = \begin{pmatrix} \hat{\varphi}_e^n \\ \hat{\varphi}_i^n \\ \hat{\psi}_e^n \end{pmatrix} = \begin{pmatrix} \frac{1}{\mu(\lambda_n)}\left[\mathcal{M}_n^{ee}(r;a_e) - \nu_n\mathcal{M}_n^{ei}(r;a_i)\right] \\ \frac{1}{\tau\lambda_n+1}\left[\mathcal{M}_n^{ie}(r;a_e) - \nu_n\mathcal{M}_n^{ii}(r;a_i)\right] \\ \frac{\alpha}{\lambda_n+\alpha}\hat{\varphi}_e^n(r) \end{pmatrix}.$$

D. Interacting pair of AE/AI/AA neural fields

The two cases of symmetric and asymmetric couplings in Eqs. (4) and (5) are treated separately below.

Case I: Symmetric case

A stationary bump solution to neural field equation (4) with the same radii a in each population can be expressed as $(u_1, u_2, n_1, n_2) = (U(r), V(r), N(r), M(r))$, where

$$\begin{aligned}
(1+\beta)U(r) &= W^{\mathrm{loc}}(r;a) + W^{\mathrm{lay}}(r;a) + I(r), \\
M(r) &= N(r) = V(r) = U(r),
\end{aligned}$$

and a satisfies the threshold condition

$$W^{\mathrm{loc}}(a;a) + W^{\mathrm{lay}}(a;a) + I(a) = \theta(1+\beta)$$

provided the threshold behavior is obeyed on $(0, \infty)$.

Time-dependent perturbations $(\widetilde{\varphi}_1, \widetilde{\varphi}_2, \widetilde{\psi}_1, \widetilde{\psi}_2)(\mathbf{r}, t)$ of stationary bump $(U(r), V(r), N(r), M(r))$ evolve according to

$$\begin{aligned}
\frac{\partial\widetilde{\varphi}_1}{\partial t} + \widetilde{\varphi}_1 &= \mathcal{N}^{\mathrm{loc}}\widetilde{\varphi}_1 + \mathcal{N}^{\mathrm{lay}}\widetilde{\varphi}_2 - \beta\widetilde{\psi}_1, \\
\frac{\partial\widetilde{\varphi}_2}{\partial t} + \widetilde{\varphi}_2 &= \mathcal{N}^{\mathrm{loc}}\widetilde{\varphi}_2 + \mathcal{N}^{\mathrm{lay}}\widetilde{\varphi}_1 - \beta\widetilde{\psi}_2, \\
\frac{1}{\alpha}\frac{\partial\widetilde{\psi}_1}{\partial t} + \widetilde{\psi}_1 &= \widetilde{\varphi}_1, \\
\frac{1}{\alpha}\frac{\partial\widetilde{\psi}_2}{\partial t} + \widetilde{\psi}_2 &= \widetilde{\varphi}_2,
\end{aligned} \tag{40}$$

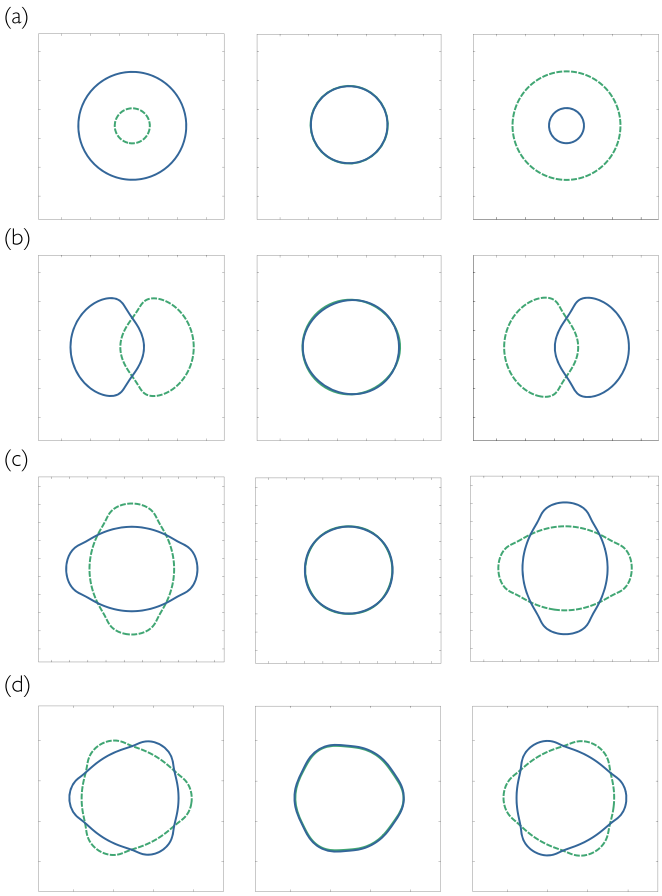

FIG. 6. Examples of n-fold *breathers* or standing waves in the interacting pair of symmetric E-I neural fields at different points in t as a result of the destabilization of a stationary bump solution via Hopf bifurcation with respect to eigenmodes with different spatial structure. The *in-phase* (not shown) and *anitphase* (shown) periodic solutions occur when the $\mathbf{\Lambda}_n^+$ and $\mathbf{\Lambda}_n^-$ modes destabilize, respectively. (a) destabilization of the $n=0$ mode leading to a radially symmetric antiphase breather; (b) destabilization of the $n=1$ mode leading to a onefold antiphase breather with D_1 dihedral symmetry; (c) destabilization of the $n=2$ mode leading to a twofold antiphase breather with D_2 dihedral symmetry; (d) destabilization of the $n=3$ mode leading to a threefold antiphase breather with D_3 dihedral symmetry. Solid and dashed curves represent the threshold boundary in layers I and II.

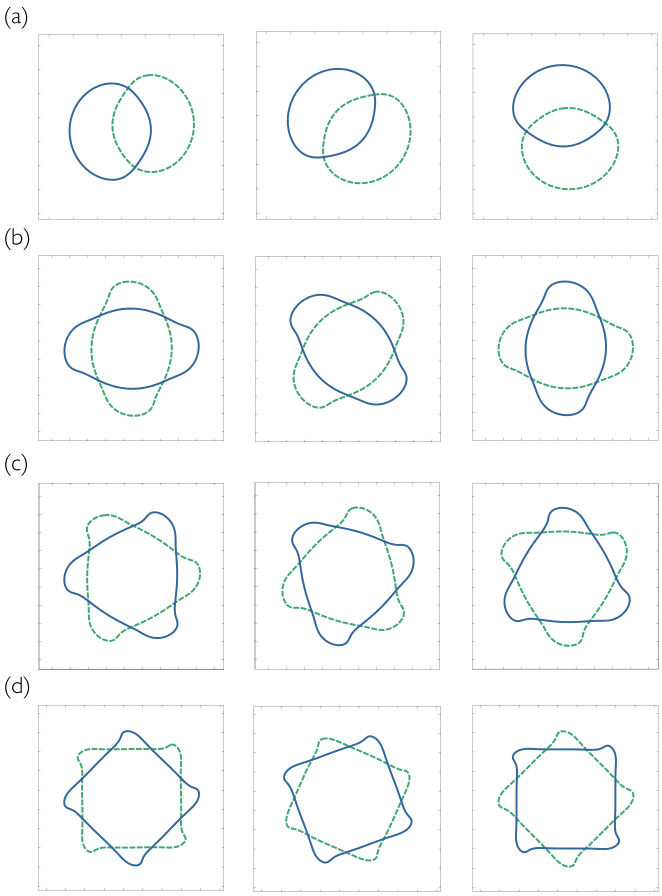

FIG. 7. Examples of n-fold *rotors* or rotating waves in the interacting pair of symmetric E-I neural fields at different points in t as a result of the destabilization of a radially symmetric stationary bump via Hopf bifurcation with respect to different spatial eigenmodes. Both *in-phase* (not shown) and *anitphase* (shown) periodic solutions occur when the $\mathbf{\Lambda}_n^+$ and $\mathbf{\Lambda}_n^-$ modes destabilize respectively. (a) Destabilization of the $n=1$ mode leading to a onefold antiphase rotor with Z_1 rotational symmetry; (b) destabilization of the $n=2$ mode leading to a twofold antiphase rotor with Z_2 rotational symmetry; (c) destabilization of the $n=3$ mode leading to a threefold antiphase rotor with Z_3 rotational symmetry; (d) destabilization of the $n=4$ mode leading to a fourfold antiphase rotor with Z_4 rotational symmetry. Solid and dashed curves represent the threshold boundary in layers I and II.

where $(\widetilde{\varphi}_1, \widetilde{\varphi}_2, \widetilde{\psi}_1, \widetilde{\psi}_2) = \boldsymbol{\varphi}(\mathbf{r})e^{\lambda t}$ leads to the spectral problem for λ and $\boldsymbol{\varphi}(\mathbf{r}) = (\varphi_1(\mathbf{r}), \varphi_2(\mathbf{r}), \psi_1(\mathbf{r}), \psi_2(\mathbf{r}))$:

$$\begin{aligned} -\varphi_1 + \mathcal{N}^{\text{loc}}\varphi_1 + \mathcal{N}^{\text{lay}}\varphi_2 - \beta\psi_1 &= \lambda\varphi_1, \\ -\varphi_2 + \mathcal{N}^{\text{loc}}\varphi_2 + \mathcal{N}^{\text{lay}}\varphi_1 - \beta\psi_2 &= \lambda\varphi_2, \\ \alpha\varphi_1 - \alpha\psi_1 &= \lambda\psi_1, \\ \alpha\varphi_2 - \alpha\psi_2 &= \lambda\psi_2. \end{aligned} \tag{41}$$

Setting $\varphi_1(r,\theta) = \hat{\varphi}_1(r)e^{in\theta}$ and $\varphi_2(r,\theta) = \hat{\varphi}_2(r)e^{in\theta}$ and

$$\psi_1(r,\theta) = \left(\frac{\alpha}{\lambda+\alpha}\right)\varphi_1(r,\theta),$$

$$\psi_2(r,\theta) = \left(\frac{\alpha}{\lambda+\alpha}\right)\varphi_2(r,\theta).$$

The compatibility equation determining the eigenvalues and special nonlocal values of the eigenfunctions of the nth eigenmode at the common threshold point $r=a$ is

$$\left(\mathbf{M}_n^{\text{SYM}} - \mathbf{I}\right)\boldsymbol{\phi}_n = \left(\lambda + \frac{\alpha\beta}{\lambda+\alpha}\right)\boldsymbol{\phi}_n, \tag{42}$$

where

$$\mathbf{M}_n^{\text{SYM}} = \begin{bmatrix} \mathcal{M}_n^{\text{loc}}(a;a) & \mathcal{M}_n^{\text{lay}}(a;a) \\ \mathcal{M}_n^{\text{lay}}(a;a) & \mathcal{M}_n^{\text{loc}}(a;a) \end{bmatrix}, \quad \boldsymbol{\phi}_n = \begin{pmatrix} \hat{\varphi}_1(a) \\ \hat{\varphi}_2(a) \end{pmatrix},$$

and $\mathcal{M}_n^l(a;a) = \Omega_n^l(a;a)/|U'(a)|$. $\mathbf{M}_n^{\text{SYM}}$ is symmetric and can be diagonalized by the similarity transformation

$$\mathbf{Q}^{-1}\mathbf{M}_n^{\text{SYM}}\mathbf{Q} = \mathbf{\Lambda}_{\text{SYM}} \equiv \begin{bmatrix} \mathcal{M}_n^+ & 0 \\ 0 & \mathcal{M}_n^- \end{bmatrix}, \quad \mathbf{Q} = \begin{bmatrix} 1 & 1 \\ 1 & -1 \end{bmatrix},$$

where $\mathcal{M}_n^{\pm} = \mathcal{M}_n^{\text{loc}}(a;a) \pm \mathcal{M}_n^{\text{lay}}(a;a)$. Compatibility equation (42) can be rewritten as

$$\left(\mathbf{M}_n^{\text{SYM}} - \mu(\lambda)\mathbf{I}\right)\boldsymbol{\phi}_n = 0, \tag{43}$$

where $\mu(\lambda) = 1 + \lambda + \frac{\alpha\beta}{\lambda+\alpha}$. Nontrivial $\boldsymbol{\phi}_n$ exist when $\det(\mathbf{M}_n^{\text{SYM}} - \mu(\lambda)\mathbf{I}) = 0$. Solving for μ and then λ in terms of μ we obtain

$$\lambda_n^{\pm} = -\Gamma \pm \sqrt{\Gamma^2 - \Delta}, \qquad \Gamma = \tfrac{1}{2}(1 + \alpha - \mu_n^{\pm}),$$
$$\mu_n^{\pm} = \mathcal{M}_n^{\text{loc}}(a;a) \pm \mathcal{M}_n^{\text{lay}}(a;a), \qquad \Delta = \alpha(1 + \beta - \mu_n^{\pm}).$$

Solving Eq. (43) for the vector of special nonlocal values we obtain the form $\boldsymbol{\phi}_n^{\pm} = (\hat{\varphi}_1(a), \hat{\varphi}_2(a)) = (1, \pm 1)$ where the $\pm$ corresponds to the different spatial modes $\mathcal{M}_n^{\pm}$. There are two nth spatial eigenmodes corresponding to μ_n^+ or μ_n^-. Spatial eigenfunctions $\boldsymbol{\varphi}_n(r,\theta)$ for an eigenvalue λ in the nth eigenmode are given by

$$\boldsymbol{\varphi}_n^1(r,\theta) = \hat{\boldsymbol{\varphi}}_n(r)e^{in\theta},$$
$$\boldsymbol{\varphi}_n^2(r,\theta) = \hat{\boldsymbol{\varphi}}_n(r)e^{-in\theta},$$

where for the *in-phase mode* (+) and *antiphase mode* (-)

$$\hat{\boldsymbol{\varphi}}_n^{\pm}(r) = \begin{pmatrix} \hat{\varphi}_1^n \\ \hat{\varphi}_2^n \\ \hat{\psi}_1^n \\ \hat{\psi}_2^n \end{pmatrix} = \begin{pmatrix} 1 \\ \pm 1 \\ \frac{\alpha}{\lambda_n^{\pm}+\alpha} \\ \frac{\pm\alpha}{\lambda_n^{\pm}+\alpha} \end{pmatrix} \left(\mathcal{M}_n^{\text{loc}}(r;a) \pm \mathcal{M}_n^{\text{lay}}(r;a)\right).$$

Although the eigenfunctions are complex-valued, we can see whether the components of the eigenfunctions associated with the two neural field layers are aligned (+) and in-phase or opposite (−) and antiphase. At a Hopf bifurcation point the Hopf frequency is

$$\omega_H = \text{Im}\{\lambda_n^{\pm}\} = \sqrt{\alpha(\beta - \alpha)}.$$

Condition for Hopf bifurcation of μ_n^+ or μ_n^- mode

If we assume that a stationary bump is stable, that both λ_n^+ and λ_n^- are complex, and one of the two nth eigenmodes destabilizes in a Hopf bifurcation, then the condition determining whether the μ_n^+ or μ_n^- eigenmode destabilizes is determined by the pair of eigenvalues whose real part is nearer to 0. In this case we have

$$\mathcal{R}\text{e}\{\lambda_n^+\} - \mathcal{R}\text{e}\{\lambda_n^-\} = \tfrac{1}{2}(\mu_n^+ - \mu_n^-) = \mathcal{M}_n^{\text{lay}}(a;a).$$

So, when $\mathcal{M}_n^{\text{lay}}(a;a) > 0$ at the Hopf bifurcation point, $\mathcal{R}\text{e}\{\lambda_n^+\} > \mathcal{R}\text{e}\{\lambda_n^-\}$ and *in-phase mode* μ_n^+ destabilizes in a Hopf bifurcation. When $\mathcal{M}_n^{\text{lay}}(a;a) < 0$ at the Hopf bifurcation point, then *antiphase mode* μ_n^- destabilizes in a Hopf bifurcation.

Case II: Asymmetric case

A stationary bump solution to neural field (5) with different radii a_1 and a_2 in each population can be expressed as $(u_1, u_2, n_1, n_2) = (U_1(r), U_2(r), N_1(r), N_2(r))$, where

$$\begin{aligned}(1+\beta)U_1(r) &= W_{11}^{\text{loc}}(r;a_1) + W_{12}^{\text{lay}}(r;a_2) + I_1(r),\\ (1+\beta)U_2(r) &= W_{22}^{\text{loc}}(r;a_2) + W_{21}^{\text{lay}}(r;a_1) + I_2(r),\\ N_1(r) &= U_1(r),\\ N_2(r) &= U_2(r),\end{aligned}$$

and a_1 and a_2 satisfy the threshold condition

$$\begin{aligned}W_{11}^{\text{loc}}(a_1;a_1) + W_{12}^{\text{lay}}(a_1;a_2) + I_1(a_1) &= \theta_1(1+\beta)\\ W_{22}^{\text{loc}}(a_2;a_2) + W_{21}^{\text{lay}}(a_2;a_1) + I_2(a_2) &= \theta_2(1+\beta)\end{aligned}$$

provided the threshold behavior is obeyed on $(0,\infty)$.

Time-dependent perturbations $(\widetilde{\varphi}_1, \widetilde{\varphi}_2, \widetilde{\psi}_1, \widetilde{\psi}_2)(\mathbf{r},t)$ of the stationary bump $(U_1(r), U_2(r), N_1(r), N_2(r))$ evolve according to

$$\begin{aligned}\frac{\partial\widetilde{\varphi}_1}{\partial t} + \widetilde{\varphi}_1 &= \mathcal{N}_{11}^{\text{loc}}\widetilde{\varphi}_1 + \mathcal{N}_{12}^{\text{lay}}\widetilde{\varphi}_2 - \beta\widetilde{\psi}_1,\\ \frac{\partial\widetilde{\varphi}_2}{\partial t} + \widetilde{\varphi}_2 &= \mathcal{N}_{22}^{\text{loc}}\widetilde{\varphi}_2 + \mathcal{N}_{21}^{\text{lay}}\widetilde{\varphi}_1 - \beta\widetilde{\psi}_2,\\ \frac{1}{\alpha}\frac{\partial\widetilde{\psi}_1}{\partial t} + \widetilde{\psi}_1 &= \widetilde{\varphi}_1,\\ \frac{1}{\alpha}\frac{\partial\widetilde{\psi}_2}{\partial t} + \widetilde{\psi}_2 &= \widetilde{\varphi}_2,\end{aligned} \tag{44}$$

where $(\widetilde{\varphi}_1, \widetilde{\varphi}_2, \widetilde{\psi}_1, \widetilde{\psi}_2) = \boldsymbol{\varphi}(\mathbf{r})e^{\lambda t}$ yields the spectral problem for λ and $\boldsymbol{\varphi}(\mathbf{r}) = (\varphi_1(\mathbf{r}), \varphi_2(\mathbf{r}), \psi_1(\mathbf{r}), \psi_2(\mathbf{r}))$:

$$\begin{aligned}-\varphi_1 + \mathcal{N}_{11}^{\text{loc}}\varphi_1 + \mathcal{N}_{12}^{\text{lay}}\varphi_2 - \beta\psi_1 &= \lambda\varphi_1,\\ -\varphi_2 + \mathcal{N}_{22}^{\text{loc}}\varphi_2 + \mathcal{N}_{21}^{\text{lay}}\varphi_1 - \beta\psi_2 &= \lambda\varphi_2,\\ \alpha\varphi_1 - \alpha\psi_1 &= \lambda\psi_1,\\ \alpha\varphi_2 - \alpha\psi_2 &= \lambda\psi_2.\end{aligned} \tag{45}$$

Setting $\varphi_1(r,\theta) = \hat{\varphi}_1(r)e^{in\theta}$ and $\varphi_2(r,\theta) = \hat{\varphi}_2(r)e^{in\theta}$, the compatibility equation determining the eigenvalues and special nonlocal values of the eigenfunctions of the nth eigenmode at threshold points a_1 and a_2 is

$$\left(\mathbf{M}_n^{\text{ASYM}} - \mathbf{I}\right)\boldsymbol{\phi}_n = \left(\lambda + \frac{\alpha\beta}{\lambda+\alpha}\right)\boldsymbol{\phi}_n, \tag{46}$$

where

$$\mathbf{M}_n^{\text{ASYM}} = \begin{bmatrix} \mathcal{M}_n^{11}(a_1;a_1) & \mathcal{M}_n^{12}(a_1;a_2) \\ \mathcal{M}_n^{21}(a_2;a_1) & \mathcal{M}_n^{22}(a_2;a_2) \end{bmatrix}, \quad \boldsymbol{\phi}_n = \begin{pmatrix} \hat{\varphi}_1(a_1) \\ \hat{\varphi}_2(a_2) \end{pmatrix}$$

and $\mathcal{M}_n^{jk}(a_j;a_k) = \Omega_n^{jk}(a_j;a_k)/|U_k'(a_k)|$. Compatibility equation (46) can be rewritten as

$$\left(\mathbf{M}_n^{\text{ASYM}} - \mu(\lambda)\mathbf{I}\right)\boldsymbol{\phi}_n = 0, \tag{47}$$

where $\mu(\lambda) = 1 + \lambda + \frac{\alpha\beta}{\lambda+\alpha}$. For nontrivial values $\boldsymbol{\phi}_n$ to Eq. (47) exist, we require $\det(\mathbf{M}_n^{\text{ASYM}} - \mu(\lambda_n)\mathbf{I}) = 0$. Solving for

μ and then solving for λ in terms of μ we obtain

$$\lambda_n^{\pm} = -\Gamma \pm \sqrt{\Gamma^2 - \Delta},$$
$$\Gamma = \tfrac{1}{2}\big(1+\alpha-\mu_n^{\pm}\big), \qquad \Delta = \alpha\big(1+\beta-\mu_n^{\pm}\big),$$
$$\mu_n^{\pm} = \left[\tfrac{\mathcal{M}_n^{11}+\mathcal{M}_n^{22}}{2}\right] \pm \sqrt{\left[\tfrac{\mathcal{M}_n^{11}-\mathcal{M}_n^{22}}{2}\right]^2 + \mathcal{M}_n^{12}\mathcal{M}_n^{21}},$$

where $\mathcal{M}_n^{jk} = \mathcal{M}_n^{jk}(a_j;a_k)$. This defines two pairs of eigenvalues $\lambda_n^{\pm}$ corresponding to spatial eigenmodes $\mu_n^{\pm}$. We note that the condition for $\mu_n^{\pm}$ to be complex is

$$\mathcal{M}_n^{12}(a_1;a_2)\,\mathcal{M}_n^{21}(a_2;a_1) < -\left[\frac{\mathcal{M}_n^{11}(a_1;a_1)-\mathcal{M}_n^{22}(a_2;a_2)}{2}\right]^2,$$

requiring either $\mathcal{M}_n^{12}(a_1;a_2)$ or $\mathcal{M}_n^{21}(a_2;a_1)$ be negative. Solving Eq. (47) for the vector of special nonlocal values $\boldsymbol{\phi}_n = (\hat{\varphi}_1(a_1), \hat{\varphi}_2(a_2)) = (1, \nu_n^{\pm})$ we obtain

$$\nu_n^{\pm} = \frac{\mu_n^{\pm} - \mathcal{M}_n^{11}(a_1;a_1)}{\mathcal{M}_n^{12}(a_1;a_2)} = \frac{\left[\frac{\mathcal{M}_n^{11}-\mathcal{M}_n^{22}}{2}\right] \pm \sqrt{\left[\frac{\mathcal{M}_n^{11}-\mathcal{M}_n^{22}}{2}\right]^2 + \mathcal{M}_n^{12}\mathcal{M}_n^{21}}}{\mathcal{M}_n^{12}},$$

where superscript $\pm$ corresponds spatial modes $\mu_n^{\pm}$.

Spatial eigenfunctions $\boldsymbol{\varphi}_n(r,\theta)$ for an eigenvalue λ in the nth eigenmode are given by

$$\boldsymbol{\varphi}_n^1(r,\theta) = \hat{\boldsymbol{\varphi}}_n(r)e^{in\theta}, \quad \boldsymbol{\varphi}_n^2(r,\theta) = \hat{\boldsymbol{\varphi}}_n(r)e^{-in\theta},$$

where radial component corresponding to $\mu_n^{\pm}$ is given by

$$\hat{\boldsymbol{\varphi}}_n^{\pm}(r) = \begin{pmatrix} \hat{\varphi}_1^n(r) \\ \hat{\varphi}_2^n(r) \\ \hat{\psi}_1^n(r) \\ \hat{\psi}_2^n(r) \end{pmatrix} = \begin{pmatrix} \mathcal{M}_n^{11}(r;a_1) + \nu_n^{\pm}\mathcal{M}_n^{12}(r;a_2) \\ \nu_n^{\pm}\mathcal{M}_n^{22}(r;a_2) + \mathcal{M}_n^{21}(r;a_1) \\ \frac{\alpha}{\lambda_n^{\pm}+\alpha}\hat{\varphi}_1^n(r) \\ \frac{\alpha}{\lambda_n^{\pm}+\alpha}\hat{\varphi}_2^n(r) \end{pmatrix}.$$

At a Hopf bifurcation point the Hopf frequency is

$$\omega_H = \mathsf{Im}\{\lambda_n^{\pm}\} = \sqrt{\alpha(\beta-\alpha)}.$$

E. Interacting pair of E-I neural fields

A stationary bump to neural field equation (6) can be expressed as $(u_e, u_i, v_e, v_i) = (U_e(r), U_i(r), V_e(r), V_i(r))$ where the solution is identical in each neural field layer and expressed as

$$\begin{aligned} U_e(r) &= W_{ee}^{\rm loc}(r;a_e) - W_{ei}^{\rm loc}(r;a_i) + W_{ee}^{\rm lay}(r;a_e) + I_e(r), \\ U_i(r) &= W_{ie}^{\rm loc}(r;a_e) - W_{ii}^{\rm loc}(r;a_i) + W_{ie}^{\rm lay}(r;a_e) + I_i(r), \\ V_e(r) &= U_e(r), \\ V_i(r) &= U_i(r), \end{aligned}$$

where the radii of the bumps in the E- and I-populations a_e and a_i satisfy the threshold conditions

$$\begin{aligned} W_{ee}^{\rm loc}(a_e;a_e) - W_{ei}^{\rm loc}(a_e;a_i) + W_{ee}^{\rm lay}(a_e;a_e) + I_e(a_e) &= \theta_e, \\ W_{ie}^{\rm loc}(a_i;a_e) - W_{ii}^{\rm loc}(a_i;a_i) + W_{ie}^{\rm lay}(a_i;a_e) + I_i(a_i) &= \theta_i. \end{aligned}$$

Time-dependent perturbations $(\widetilde{\varphi}_e, \widetilde{\varphi}_i, \widetilde{\psi}_e, \widetilde{\psi}_i)(\mathbf{r},t)$ of the stationary bump $(U_e(r), U_i(r), V_e(r), V_i(r))$ evolve according to

$$\begin{aligned} \frac{\partial\widetilde{\varphi}_e}{\partial t} + \widetilde{\varphi}_e &= \mathcal{N}_{ee}^{\rm loc}\widetilde{\varphi}_e - \mathcal{N}_{ei}^{\rm loc}\widetilde{\varphi}_i + \mathcal{N}_{ee}^{\rm lay}\widetilde{\psi}_e, \\ \tau\frac{\partial\widetilde{\varphi}_i}{\partial t} + \widetilde{\varphi}_i &= \mathcal{N}_{ie}^{\rm loc}\widetilde{\varphi}_e - \mathcal{N}_{ii}^{\rm loc}\widetilde{\varphi}_i + \mathcal{N}_{ie}^{\rm lay}\widetilde{\psi}_e, \\ \frac{\partial\widetilde{\psi}_e}{\partial t} + \widetilde{\psi}_e &= \mathcal{N}_{ee}^{\rm loc}\widetilde{\psi}_e - \mathcal{N}_{ei}^{\rm loc}\widetilde{\psi}_i + \mathcal{N}_{ee}^{\rm lay}\widetilde{\varphi}_e, \\ \tau\frac{\partial\widetilde{\psi}_i}{\partial t} + \widetilde{\psi}_i &= \mathcal{N}_{ie}^{\rm loc}\widetilde{\psi}_e - \mathcal{N}_{ii}^{\rm loc}\widetilde{\psi}_i + \mathcal{N}_{ie}^{\rm lay}\widetilde{\varphi}_e, \end{aligned} \tag{48}$$

where $(\widetilde{\varphi}_e, \widetilde{\varphi}_i, \widetilde{\psi}_e, \widetilde{\psi}_i) = \boldsymbol{\varphi}(\mathbf{r})e^{\lambda t}$ results in the spectral problem for λ and $\boldsymbol{\varphi}(\mathbf{r}) = (\varphi_e(\mathbf{r}), \varphi_i(\mathbf{r}), \psi_e(\mathbf{r}), \psi_i(\mathbf{r}))$:

$$\begin{aligned} -\varphi_e + \mathcal{N}_{ee}^{\rm loc}\varphi_e - \mathcal{N}_{ei}^{\rm loc}\varphi_i + \mathcal{N}_{ee}^{\rm lay}\psi_e &= \lambda\varphi_e, \\ -\frac{1}{\tau}\varphi_i + \frac{1}{\tau}\mathcal{N}_{ie}^{\rm loc}\varphi_e - \frac{1}{\tau}\mathcal{N}_{ii}^{\rm loc}\varphi_i + \frac{1}{\tau}\mathcal{N}_{ie}^{\rm lay}\psi_e &= \lambda\varphi_i, \\ -\psi_e + \mathcal{N}_{ee}^{\rm loc}\psi_e - \mathcal{N}_{ei}^{\rm loc}\psi_i + \mathcal{N}_{ee}^{\rm lay}\varphi_e &= \lambda\psi_e, \\ -\frac{1}{\tau}\psi_i + \frac{1}{\tau}\mathcal{N}_{ie}^{\rm loc}\psi_e - \frac{1}{\tau}\mathcal{N}_{ii}^{\rm loc}\psi_i + \frac{1}{\tau}\mathcal{N}_{ie}^{\rm lay}\varphi_e &= \lambda\psi_i. \end{aligned} \tag{49}$$

The compatibility equation determining the eigenvalues and special nonlocal values of the eigenfunctions of the nth eigenmode at threshold points $r = a_e$ and a_i is

$$\big(\mathbf{M}_n^{\rm dual} - \mathbf{I}_{\rm dual}\big)\boldsymbol{\phi}_n = \lambda\,\boldsymbol{\phi}_n. \tag{50}$$

$\mathbf{I}_{\rm dual} = \mathsf{diag}\,(1,\ \tau^{-1},\ 1,\ \tau^{-1})$ and $\mathbf{M}_n^{\rm dual}$ is a (4×4) matrix $\boldsymbol{\phi}_n = (\hat{\varphi}_e(a_e), \hat{\varphi}_i(a_i), \hat{\psi}_e(a_e), \hat{\psi}_i(a_i))$ and

$$\mathbf{M}_n^{\rm dual} = \begin{bmatrix} \mathbf{M}_n^{\rm EI} & \mathbf{M}_n^{\rm lay} \\ \mathbf{M}_n^{\rm lay} & \mathbf{M}_n^{\rm EI} \end{bmatrix}, \quad \mathbf{M}_n^{\rm lay} = \begin{bmatrix} \mathcal{M}_{n,ee}^{\rm lay}(a_e;a_e) & 0 \\ \frac{1}{\tau}\mathcal{M}_{n,ie}^{\rm lay}(a_i;a_e) & 0 \end{bmatrix},$$

$$\mathbf{M}_n^{\rm EI} = \begin{bmatrix} \mathcal{M}_n^{ee}(a_e;a_e) & -\mathcal{M}_n^{ei}(a_e;a_i) \\ \frac{1}{\tau}\mathcal{M}_n^{ie}(a_i;a_e) & -\frac{1}{\tau}\mathcal{M}_n^{ii}(a_i;a_i) \end{bmatrix},$$

where $\mathcal{M}_n^{jk}(a_j;a_k) = \Omega_n^{jk}(a_j;a_k)/|U_k'(a_k)|$ and similarly $\mathcal{M}_{n,jk}^{\rm lay}(a_j;a_k) = \Omega_{n,jk}^{\rm lay}(a_j;a_k)/|U_k'(a_k)|$. $\mathbf{M}_n^{\rm dual}$ is block diagonalized by a similarity transformation as follows:

$$\mathbf{Q}^{-1}\mathbf{M}_n^{\rm dual}\mathbf{Q} = \boldsymbol{\Lambda}_{\rm dual} \equiv \begin{bmatrix} \boldsymbol{\Lambda}_n^{+} & 0 \\ 0 & \boldsymbol{\Lambda}_n^{-} \end{bmatrix}, \ \mathbf{Q} = \begin{bmatrix} \mathrm{I}_2 & \mathrm{I}_2 \\ \mathrm{I}_2 & -\mathrm{I}_2 \end{bmatrix},$$

where

$$\boldsymbol{\Lambda}_n^{\pm} = \begin{bmatrix} \mathcal{M}_n^{ee}(a_e;a_e) \pm \mathcal{M}_{n,ee}^{\rm lay}(a_e;a_e) & -\mathcal{M}_n^{ei}(a_e;a_i) \\ \frac{1}{\tau}\mathcal{M}_n^{ie}(a_i;a_e) \pm \frac{1}{\tau}\mathcal{M}_{n,ie}^{\rm lay}(a_i;a_e) & -\frac{1}{\tau}\mathcal{M}_n^{ii}(a_i;a_i) \end{bmatrix}.$$

Nontrivial values $\boldsymbol{\phi}_n$ exist if $\det(\mathbf{M}_n^{\rm dual} - \mathbf{I}_{\rm dual} - \lambda\mathbf{I}) = 0$. Solving for λ results in two pairs of eigenvalues corresponding to the spatial eigenmodes associated with $\boldsymbol{\Lambda}_n^{\pm}$

$$\lambda_n^{\pm} = \left[\tfrac{\mathcal{M}_{n,ee}^{\pm}-1}{2} - \tfrac{\mathcal{M}_n^{ii}+1}{2\tau}\right] \pm \sqrt{\left[\tfrac{\mathcal{M}_{n,ee}^{\pm}-1}{2} + \tfrac{\mathcal{M}_n^{ii}+1}{2\tau}\right]^2 - \tfrac{\mathcal{M}_n^{ei}\mathcal{M}_{n,ie}^{\pm}}{\tau}},$$

where $\mathcal{M}_{n,jk}^{\pm}(a_j;a_k) = \mathcal{M}_n^{jk}(a_j;a_k) \pm \mathcal{M}_{n,jk}^{\rm lay}(a_j;a_k)$. The vector of special nonlocal values in the form

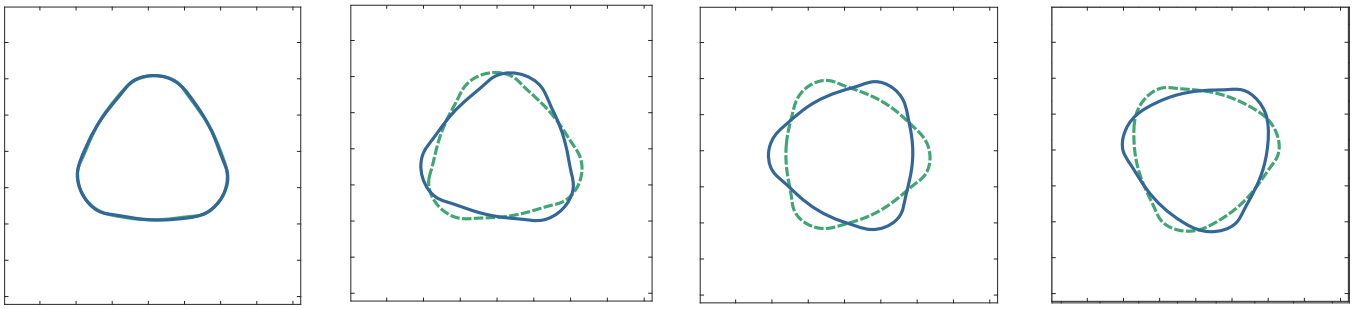

FIG. 8. Threefold *antidirectional* rotor in the interacting pair of E-I neural fields where the rotors in the E populations in layer I (solid blue curve) and layer II (dashed green curve) rotate in opposite directions. Plotted curves indicate the threshold boundary of the superthreshold region at different points in time t. This is an example of a periodic solution that occurs well beyond a Hopf bifurcation point.

$\boldsymbol{\phi}_n = (\hat{\varphi}_e(a_e), \hat{\varphi}_i(a_i), \hat{\psi}_e(a_e), \hat{\psi}_i(a_i)) = (1, \nu_n^{\pm}, \pm 1, \pm\nu_n^{\pm})$ is

$$\nu_n^{\pm} = \frac{\lambda_n^{\pm} + 1 - \mathcal{M}_{n,ee}^{\pm}(a_e; a_e)}{-\mathcal{M}_n^{ei}(a_e; a_i)}.$$

Spatial eigenfunctions for the nth eigenmode are

$$\boldsymbol{\varphi}_n^1(r,\theta) = \hat{\boldsymbol{\varphi}}_n(r)e^{in\theta}, \quad \boldsymbol{\varphi}_n^2(r,\theta) = \hat{\boldsymbol{\varphi}}_n(r)e^{-in\theta}.$$

The spatial eigenmodes corresponding to $\boldsymbol{\Lambda}_n^+$ and $\boldsymbol{\Lambda}_n^-$ are the *in-phase mode* $(+)$ and *antiphase mode* $(-)$ where

$$\hat{\boldsymbol{\varphi}}_n^{\pm}(r) = \begin{pmatrix} \frac{1}{\lambda_n^+ + 1}\left[\mathcal{M}_{n,ee}^{\pm}(r; a_e) - \nu_n^{\pm}\mathcal{M}_n^{ei}(r; a_i)\right] \\ \frac{1}{\tau\lambda_n^+ + 1}\left[\mathcal{M}_{n,ie}^{\pm}(r; a_e) - \nu_n^{\pm}\mathcal{M}_n^{ii}(r; a_i)\right] \\ \pm\frac{1}{\lambda_n^+ + 1}\left[\mathcal{M}_{n,ee}^{\pm}(r; a_e) - \nu_n^{\pm}\mathcal{M}_n^{ei}(r; a_i)\right] \\ \pm\frac{1}{\tau\lambda_n^+ + 1}\left[\mathcal{M}_{n,ie}^{\pm}(r; a_e) - \nu_n^{\pm}\mathcal{M}_n^{ii}(r; a_i)\right] \end{pmatrix}.$$

At a Hopf bifurcation point the Hopf frequency is

$$\omega_H = \mathsf{Im}\{\lambda_n^{\pm}\} = \sqrt{\frac{-(\mathcal{M}_{n,ee}^{\pm} - 1)(\mathcal{M}_n^{ii} + 1) + \mathcal{M}_n^{ei}\mathcal{M}_{n,ie}^{\pm}}{\tau}},$$

where $(\mathcal{M}_{n,ee}^{\pm} - 1) = (\mathcal{M}_n^{ii} + 1)/\tau$.

Condition for Hopf bifurcation of the $\boldsymbol{\Lambda}_n^{\pm}$ mode

If we assume that a stationary bump is stable, that both λ_n^+ and λ_n^- are complex, and one of the two nth eigenmodes destabilizes in a Hopf bifurcation, then the condition determining if the $\boldsymbol{\Lambda}_n^+$ or $\boldsymbol{\Lambda}_n^-$ eigenmode destabilizes is determined by the eigenvalues with real part closer to 0:

$$\mathcal{R}\mathsf{e}\{\lambda_n^+\} - \mathcal{R}\mathsf{e}\{\lambda_n^-\} = \mathcal{M}_{n,ee}^{\text{lay}}(a_e; a_e).$$

When $\mathcal{M}_{n,ee}^{\text{lay}}(r; a) > 0$, *in-phase mode* $\boldsymbol{\Lambda}_n^+$ destabilizes first in the Hopf bifurcation. The *antiphase mode* $\boldsymbol{\Lambda}_n^-$ destabilizes if $\mathcal{M}_{n,ee}^{\text{lay}}(a_e; a_e) < 0$ at the bifurcation point. We assumed $w_{ee}^{\text{lay}}(r) > 0$ to represent excitatory, long-range connections [32,33]. Permitting $w_{ee}^{\text{lay}}(r) < 0$ or adding inhibitory interlayer connections introduce further means to destabilize the *antiphase mode* $\boldsymbol{\Lambda}_n^-$ mode.

Figures 6 and 7 illustrate examples of antiphase breathers and rotors with n-fold symmetry in the interacting pair of E-I neural fields. In Fig. 8 shows a solution well beyond a Hopf bifurcation point that exhibits antidirectional rotors.

F. Comment on Hopf bifurcation

We mention that the Hopf bifurcation results in this analysis should be expected to apply only in a vicinity of any supercritical Hopf bifurcation point with regard to the behavior of the emergent periodic solutions. Stable solutions far from the bifurcation point can change and behave differently due to secondary or subcritical bifurcations and other stable attractors may coexist nearby.

VII. RING SOLUTIONS IN E-I NEURAL FIELD

Ring solutions come in different forms but we briefly describe two examples encountered in the E-I neural field that underwent Hopf bifurcation. Case I is a ring in the E population with a bump in the I population. Case II is a ring in the E population with a bump surrounded by a ring in the I population.

A. Case I: Ring solution in one population only

We consider a stationary solution to E-I neural field (2) where the activity in the E-population is a radially symmetric ring with two threshold crossings at $0 < a_0^e < a_1^e$ satisfying the conditions below on $[0, \infty)$ (see Fig. 9)

$$U_e^{\text{ring}}(r) > \theta_e, \quad r \in (a_0^e, a_1^e);$$
$$U_e^{\text{ring}}(a_j^e) = \theta_e, \quad j = 0, 1;$$

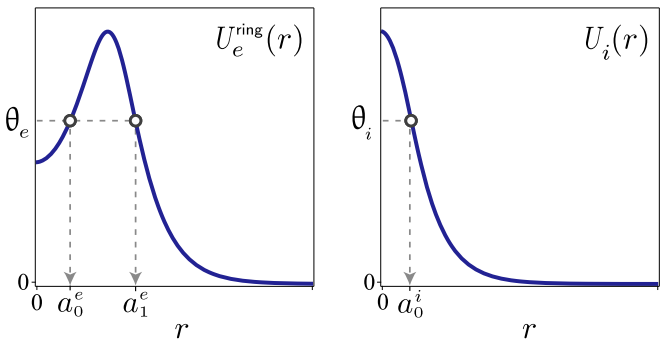

FIG. 9. Diagram of the profile of a ring solution for Case I in the E-I neural field, with a ring in the E population with threshold crossings a_0^e and a_1^e and a bump in the I population with one threshold crossing at $r = a_0^i$.

$$U_e^{\text{ring}}(r) < \theta_e, \quad r \in [0, a_0^e) \cup (a_1^e, \infty)$$
$$U_e^{\text{ring}}(r) \to 0 \ \text{ as } r \longrightarrow \infty \tag{51}$$

and the I-population is a stationary bump with a single threshold crossing at $r = a_0^i$ satisfying

$$\begin{aligned} U_i(r) &> \theta_i, \quad r \in [0, a_0^i); \\ U_i(a_0^i) &= \theta_i, \\ U_i(r) &< \theta_i, \quad r \in (a_0^i, \infty). \\ U_i(r) &\to 0 \quad \text{as } r \to \infty \end{aligned} \tag{52}$$

The synaptic terms for a ring in the E population and a bump in the I population for $j \in e, i$ are given by

$$\begin{aligned} W_{je}^{\text{ring}}(r; a_0^e, a_1^e) &= \int_{\mathbb{R}^2} w_{jk}(||\mathbf{r} - \mathbf{r}'||) H\big(U_e^{\text{ring}}(r') - \theta_e\big) d^2\mathbf{r}' \\ &= \int_0^{2\pi} \int_{a_0^e}^{a_1^e} w_{je}(||\mathbf{r} - \mathbf{r}'||) r' dr' d\theta, \\ &= W_{je}(r; a_1^e) - W_{je}(r; a_0^e), \\ W_{ji}(r; a_0^i) &= \int_{\mathbb{R}^2} w_{ji}(||\mathbf{r} - \mathbf{r}'||) H(U_i(r') - \theta_i) d^2\mathbf{r}' \\ &= \int_0^{2\pi} \int_0^{a_0^i} w_{ji}(||\mathbf{r} - \mathbf{r}'||) r' dr' d\theta. \end{aligned} \tag{53}$$

where $W_{jk}(r; a)$ was defined in Eq. (13). The ring solution (51) and (52) can accordingly be expressed in the form

$$\begin{aligned} U_e^{\text{ring}}(r) &= W_{ee}^{\text{ring}}(r; a_0^e, a_1^e) - W_{ei}(r; a_0^i) + I_e(r), \\ U_i(r) &= W_{ie}^{\text{ring}}(r; a_0^e, a_1^e) - W_{ii}(r; a_0^i) + I_i(r). \end{aligned}$$

Threshold conditions (51) and (52) can then be expressed as

$$\begin{aligned} W_{ee}^{\text{ring}}(a_0^e; a_0^e, a_1^e) - W_{ei}(a_0^e; a_0^i) + I_e(a_0^e) &= \theta_e \\ W_{ee}^{\text{ring}}(a_1^e; a_0^e, a_1^e) - W_{ei}(a_1^e; a_0^i) + I_e(a_1^e) &= \theta_e \\ W_{ie}^{\text{ring}}(a_0^i; a_0^e, a_1^e) - W_{ii}(a_0^i; a_0^i) + I_i(a_0^i) &= \theta_i \end{aligned}$$

Small perturbations $(\widetilde{\varphi}_e, \widetilde{\varphi}_i)$ to the ring solution $(U_e^{\text{ring}}(r), U_i(r))$ evolve according to

$$\begin{aligned} \frac{\partial \widetilde{\varphi}_e}{\partial t} + \widetilde{\varphi}_e &= \mathcal{N}_{ee}^{\text{ring}} \widetilde{\varphi}_e - \mathcal{N}_{ei} \widetilde{\varphi}_i, \\ \tau \frac{\partial \widetilde{\varphi}_i}{\partial t} + \widetilde{\varphi}_i &= \mathcal{N}_{ie}^{\text{ring}} \widetilde{\varphi}_e - \mathcal{N}_{ii} \widetilde{\varphi}_i. \end{aligned} \tag{54}$$

Setting $(\widetilde{\varphi}_e, \widetilde{\varphi}_i) = \boldsymbol{\varphi}(\mathbf{r}) e^{\lambda t}$ leads to the spectral problem for λ and $\boldsymbol{\varphi}(\mathbf{r}) = (\varphi_e(\mathbf{r}), \varphi_i(\mathbf{r}))$:

$$\begin{aligned} -\varphi_e + \mathcal{N}_{ee}^{\text{ring}} \varphi_e - \mathcal{N}_{ei} \varphi_i &= \lambda \varphi_e, \\ -\frac{1}{\tau}\varphi_i + \frac{1}{\tau}\mathcal{N}_{ie}^{\text{ring}} \varphi_e - \frac{1}{\tau}\mathcal{N}_{ii} \varphi_i &= \lambda \varphi_i. \end{aligned} \tag{55}$$

Setting $\varphi_e(r, \theta) = \hat{\varphi}_e(r) e^{in\theta}$ and $\varphi_i(r, \theta) = \hat{\varphi}_i(r) e^{in\theta}$ the compatibility equation determining both the eigenvalues and special nonlocal values of the eigenfunctions of the nth eigenmode at threshold points a_e and a_i is given by

$$\big(\mathbf{M}_n^{\text{EIring1}} - \mathbf{I}_{\text{EIring1}}\big) \boldsymbol{\phi}_n = \lambda_n \boldsymbol{\phi}_n, \tag{56}$$

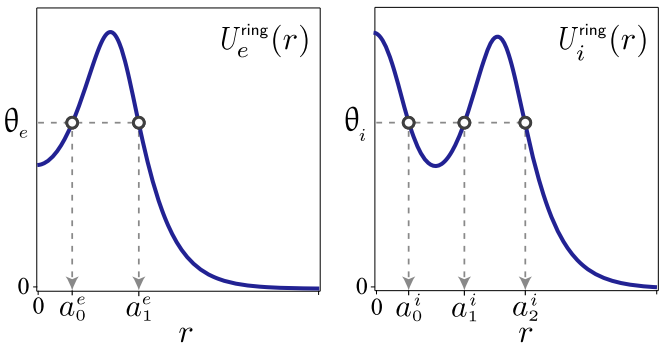

FIG. 10. Diagram of the profile of a ring solution for Case II in the E-I neural field, with a ring in the E population with threshold crossings a_0^e and a_1^e and a bump encircled by a ring in the I population with threshold points a_0^i, a_1^i, and a_2^i.

where $\mathbf{I}_{\text{EIring1}} = \text{diag}\,(1,\ 1,\ \tau^{-1})$,

$$\boldsymbol{\phi}_n = \big(\hat{\varphi}_e(a_0^e),\ \hat{\varphi}_e(a_1^e),\ \hat{\varphi}_i(a_0^i)\big),$$

and $\mathbf{M}_n^{\text{EIring1}}$ is the (3×3) matrix

$$\mathbf{M}_n^{\text{EIring1}} = \begin{bmatrix} \mathcal{M}_n^{ee}(a_0^e; a_0^e) & \mathcal{M}_n^{ee}(a_0^e; a_1^e) & -\mathcal{M}_n^{ei}(a_0^e; a_0^i) \\ \mathcal{M}_n^{ee}(a_1^e; a_0^e) & \mathcal{M}_n^{ee}(a_1^e; a_1^e) & -\mathcal{M}_n^{ei}(a_1^e; a_0^i) \\ \frac{1}{\tau}\mathcal{M}_n^{ie}(a_0^i; a_0^e) & \frac{1}{\tau}\mathcal{M}_n^{ie}(a_0^i; a_1^e) & -\frac{1}{\tau}\mathcal{M}_n^{ii}(a_0^i; a_0^i) \end{bmatrix}$$

and $\mathcal{M}_n^{jk}(a_j; a_k) = \Omega_n^{jk}(a_j; a_k)/|U_k^{\text{ring}\prime}(a_k)|$.

Accordingly eigenvalues λ_n for the nth eigenmode in the linearization about the ring solution are given by

$$\det\big(\mathbf{M}_n^{\text{EIring1}} - \mathbf{I}_{\text{EIring1}} - \lambda_n \mathbf{I}\big) = 0.$$

Consequently, the function $\mathcal{E}_n(\lambda)$ where

$$\mathcal{E}_n(\lambda) = \det\big(\mathbf{M}_n^{\text{EIring1}} - \mathbf{I}_{\text{EIring1}} - \lambda_n \mathbf{I}\big)$$

is an Evans function for the nth eigenmode of the stationary ring solution and we combine cases $n = 0, 1, 2, \ldots$. The spatial eigenfunctions $\boldsymbol{\varphi}_n(r, \theta)$ for the nth eigenmode can be expressed in a similar form as before

$$\boldsymbol{\varphi}_n^1(r, \theta) = \hat{\boldsymbol{\varphi}}_n(r) e^{in\theta}, \quad \boldsymbol{\varphi}_n^2(r, \theta) = \hat{\boldsymbol{\varphi}}_n(r) e^{-in\theta},$$

where $\hat{\boldsymbol{\varphi}}_n(r) = (\hat{\varphi}_e^n(r),\ \hat{\varphi}_i^n(r))$.

B. Case II: Ring solution in both populations

We consider a stationary solution to E-I neural field (2) where superthreshold activity in the E-population is a radially symmetric ring with two threshold crossings at $(0 < a_0^e < a_1^e)$ satisfying the following conditions on $[0, \infty)$ (see Fig. 10):

$$\begin{aligned} U_e^{\text{ring}}(r) &> \theta_e, \quad r \in (a_0^e, a_1^e); \\ U_e^{\text{ring}}(a_j^e) &= \theta_e, \quad j = 0, 1; \\ U_e^{\text{ring}}(r) &< \theta_e, \quad r \in [0, a_0^e) \cup (a_1^e, \infty) \\ U_e^{\text{ring}}(r) &\to 0 \quad \text{as } r \to \infty \end{aligned} \tag{57}$$

and the I-population is a stationary solution with three threshold crossings at radii $(0 < a_0^i < a_1^i < a_2^i)$ having the form

of an inner superthreshold bump surrounded by a concentric outer superthreshold ring satisfying

$$\begin{aligned} U_i^{\text{ring}}(r) &> \theta_i, \quad r \in [0, a_0^i) \cup (a_1^i, a_2^i); \\ U_i^{\text{ring}}(a_j^i) &= \theta_i, \quad j = 0, 1, 2; \\ U_i^{\text{ring}}(r) &< \theta_i, \quad r \in (a_0^i, a_1^i) \cup (a_2^i, \infty); \\ U_i^{\text{ring}}(r) &\to 0 \quad \text{as } r \longrightarrow \infty. \end{aligned} \tag{58}$$

The synaptic terms due to a ring in the E population and a bump encircled by a ring in the I population for $j \in e, i$ are given by

$$\begin{aligned} W_{je}^{\text{ring}}(r; a_0^e, a_1^e) &= \int_{\mathbb{R}^2} w_{jk}(||\mathbf{r} - \mathbf{r}'||) H\big(U_e^{\text{ring}}(r') - \theta_e\big) d^2\mathbf{r}' \\ &= \int_0^{2\pi} \int_{a_0^e}^{a_1^e} w_{je}(||\mathbf{r} - \mathbf{r}'||) r' dr' d\theta, \\ &= W_{je}(r; a_1^e) - W_{je}(r; a_0^e), \\ W_{ji}^{\text{ring}}(r; a_0^i, a_1^i, a_2^i) &= \int_{\mathbb{R}^2} w_{ji}(||\mathbf{r} - \mathbf{r}'||) H\big(U_i^{\text{ring}}(r') - \theta_i\big) d^2\mathbf{r}' \\ &= \int_0^{2\pi} \int_0^{a_0^i} w_{ji}(||\mathbf{r} - \mathbf{r}'||) r' dr' d\theta. \\ &+ \int_0^{2\pi} \int_{a_1^i}^{a_2^i} w_{je}(||\mathbf{r} - \mathbf{r}'||) r' dr' d\theta \\ &= W_{ji}(r; a_0^i) + W_{ji}(r; a_2^i) - W_{ji}(r; a_1^i) \end{aligned}$$

where $W_{jk}(r; a)$ was defined in Eq. (13). Consequently, the ring solution can be expressed in the form

$$\begin{aligned} U_e^{\text{ring}}(r) &= W_{ee}^{\text{ring}}(r; a_0^e, a_1^e) - W_{ei}^{\text{ring}}(r; a_0^i, a_1^i, a_2^i) + I_e(r), \\ U_i^{\text{ring}}(r) &= W_{ie}^{\text{ring}}(r; a_0^e, a_1^e) - W_{ii}^{\text{ring}}(r; a_0^i, a_1^i, a_2^i) + I_i(r). \end{aligned}$$

Threshold conditions (57) and (58) can then be expressed as

$$\begin{aligned} W_{ee}^{\text{ring}}(a_0^e; a_0^e, a_1^e) - W_{ei}^{\text{ring}}(a_0^e; a_0^i, a_1^i, a_2^i) + I_e(a_0^e) &= \theta_e \\ W_{ee}^{\text{ring}}(a_1^e; a_0^e, a_1^e) - W_{ei}^{\text{ring}}(a_1^e; a_0^i, a_1^i, a_2^i) + I_e(a_1^e) &= \theta_e \\ W_{ie}^{\text{ring}}(a_0^i; a_0^e, a_1^e) - W_{ii}^{\text{ring}}(a_0^i; a_0^i, a_1^i, a_2^i) + I_i(a_0^i) &= \theta_i \\ W_{ie}^{\text{ring}}(a_1^i; a_0^e, a_1^e) - W_{ii}^{\text{ring}}(a_1^i; a_0^i, a_1^i, a_2^i) + I_i(a_1^i) &= \theta_i \\ W_{ie}^{\text{ring}}(a_2^i; a_0^e, a_1^e) - W_{ii}^{\text{ring}}(a_2^i; a_0^i, a_1^i, a_2^i) + I_i(a_2^i) &= \theta_i \end{aligned}$$

Small perturbations $(\widetilde{\varphi}_e, \widetilde{\varphi}_i)$ to the ring solution $(U_e^{\text{ring}}(r), U_i^{\text{ring}}(r))$ evolve according to

$$\begin{aligned} \frac{\partial \widetilde{\varphi}_e}{\partial t} + \widetilde{\varphi}_e &= \mathcal{N}_{ee}^{\text{ring}} \widetilde{\varphi}_e - \mathcal{N}_{ei}^{\text{ring}} \widetilde{\varphi}_i, \\ \tau \frac{\partial \widetilde{\varphi}_i}{\partial t} + \widetilde{\varphi}_i &= \mathcal{N}_{ie}^{\text{ring}} \widetilde{\varphi}_e - \mathcal{N}_{ii}^{\text{ring}} \widetilde{\varphi}_i. \end{aligned} \tag{59}$$

Setting $(\widetilde{\varphi}_e, \widetilde{\varphi}_i) = \boldsymbol{\varphi}(\mathbf{r}) e^{\lambda t}$ leads to the spectral problem for λ and $\boldsymbol{\varphi}(\mathbf{r}) = (\varphi_e(\mathbf{r}), \varphi_i(\mathbf{r}))$:

$$\begin{aligned} -\varphi_e + \mathcal{N}_{ee}^{\text{ring}} \varphi_e - \mathcal{N}_{ei}^{\text{ring}} \varphi_i &= \lambda \varphi_e, \\ -\tfrac{1}{\tau}\varphi_i + \tfrac{1}{\tau}\mathcal{N}_{ie}^{\text{ring}} \varphi_e - \tfrac{1}{\tau}\mathcal{N}_{ii}^{\text{ring}} \varphi_i &= \lambda \varphi_i. \end{aligned} \tag{60}$$

Setting $\varphi_e(r, \theta) = \hat{\varphi}_e(r) e^{in\theta}$ and $\varphi_i(r, \theta) = \hat{\varphi}_i(r) e^{in\theta}$ the compatibility equation determining the eigenvalues and special nonlocal values of the eigenfunctions of the nth eigenmode at threshold points a_e and a_i is

$$\big(\mathbf{M}_n^{\text{EIring2}} - \mathbf{I}_{\text{EIring2}}\big)\boldsymbol{\phi}_n = \lambda_n \boldsymbol{\phi}_n, \tag{61}$$

where $\mathbf{I}_{\text{EIring2}} = \text{diag}\,(1,\ 1,\ \tau^{-1},\ \tau^{-1},\ \tau^{-1})$, and the vector $\boldsymbol{\phi}_n$ of special nonlocal values

$$\boldsymbol{\phi}_n = \big(\hat{\varphi}_e(a_0^e),\ \hat{\varphi}_e(a_1^e),\ \hat{\varphi}_i(a_0^i),\ \hat{\varphi}_i(a_1^i),\ \hat{\varphi}_i(a_2^i)\big),$$

and $\mathbf{M}_n^{\text{EIring2}}$ is the (5×5) block matrix

$$\mathbf{M}_n^{\text{EIring2}} = \begin{bmatrix} \mathbf{M}_n^{\text{ee}} & \mathbf{M}_n^{\text{ei}} \\ \mathbf{M}_n^{\text{ie}} & \mathbf{M}_n^{\text{ii}} \end{bmatrix},$$

where the block submatrices are

$$\mathbf{M}_n^{\text{ee}} = \begin{bmatrix} \mathcal{M}_n^{ee}(a_0^e; a_0^e) & \mathcal{M}_n^{ee}(a_0^e; a_1^e) \\ \mathcal{M}_n^{ee}(a_1^e; a_0^e) & \mathcal{M}_n^{ee}(a_1^e; a_1^e) \end{bmatrix},$$

$$\mathbf{M}_n^{\text{ei}} = \begin{bmatrix} -\mathcal{M}_n^{ei}(a_0^e; a_0^i) & -\mathcal{M}_n^{ei}(a_0^e; a_1^i) & -\mathcal{M}_n^{ei}(a_0^e; a_2^i) \\ -\mathcal{M}_n^{ei}(a_1^e; a_0^i) & -\mathcal{M}_n^{ei}(a_1^e; a_1^i) & -\mathcal{M}_n^{ei}(a_1^e; a_2^i) \end{bmatrix},$$

$$\mathbf{M}_n^{\text{ie}} = \begin{bmatrix} \frac{1}{\tau}\mathcal{M}_n^{ie}(a_0^i, a_0^e) & \frac{1}{\tau}\mathcal{M}_n^{ie}(a_0^i, a_1^e) \\ \frac{1}{\tau}\mathcal{M}_n^{ie}(a_1^i, a_0^e) & \frac{1}{\tau}\mathcal{M}_n^{ie}(a_1^i, a_1^e) \\ \frac{1}{\tau}\mathcal{M}_n^{ie}(a_2^i, a_0^e) & \frac{1}{\tau}\mathcal{M}_n^{ie}(a_2^i, a_1^e) \end{bmatrix},$$

$$\mathbf{M}_n^{\text{ii}} = \begin{bmatrix} -\frac{1}{\tau}\mathcal{M}_n^{ii}(a_0^i, a_0^i) & -\frac{1}{\tau}\mathcal{M}_n^{ii}(a_0^i, a_1^i) & -\frac{1}{\tau}\mathcal{M}_n^{ii}(a_0^i, a_2^i) \\ -\frac{1}{\tau}\mathcal{M}_n^{ii}(a_1^i, a_0^i) & -\frac{1}{\tau}\mathcal{M}_n^{ii}(a_1^i, a_1^i) & -\frac{1}{\tau}\mathcal{M}_n^{ii}(a_1^i, a_2^i) \\ -\frac{1}{\tau}\mathcal{M}_n^{ii}(a_2^i, a_0^i) & -\frac{1}{\tau}\mathcal{M}_n^{ii}(a_2^i, a_1^i) & -\frac{1}{\tau}\mathcal{M}_n^{ii}(a_2^i, a_2^i) \end{bmatrix},$$

and $\mathcal{M}_n^{jk}(a_j; a_k) = \Omega_n^{jk}(a_j; a_k)/|U_k^{\text{ring}\,\prime}(a_k)|$.

Accordingly, eigenvalues λ_n for the nth eigenmode in the linearization about the ring solution are solutions to

$$\det\big(\mathbf{M}_n^{\text{EIring2}} - \mathbf{I}_{\text{EIring2}} - \lambda_n \mathbf{I}\big) = 0.$$

Thus, the Evans function $\mathcal{E}_n(\lambda)$ for the nth eigenmode is

$$\mathcal{E}_n(\lambda) = \det\big(\mathbf{M}_n^{\text{EIring2}} - \mathbf{I}_{\text{EIring2}} - \lambda_n \mathbf{I}\big).$$

The spatial eigenfunctions $\boldsymbol{\varphi}_n(r, \theta)$ for the nth eigenmode can be expressed in a similar form as before,

$$\boldsymbol{\varphi}_n^1(r, \theta) = \hat{\boldsymbol{\varphi}}_n(r) e^{in\theta}, \quad \boldsymbol{\varphi}_n^2(r, \theta) = \hat{\boldsymbol{\varphi}}_n(r) e^{-in\theta},$$

where $\hat{\boldsymbol{\varphi}}_n(r) = (\hat{\varphi}_e^n(r),\ \hat{\varphi}_i^n(r))$.

Fig. 11 illustrates some examples of ring breathers and rotors with n-fold symmetry observed in the E-I neural field.

VIII. DISUCSSION

In this paper we have discussed a family of elementary neural fields whose activity is mediated by synaptic excitation and inhibition and modulated by a linear adaptation or a negative feedback gating variable and in the presence or absence of an input homogeneity on two-dimensional domain $\mathbb{R}^2$. For each of these elementary neural field models, the linear stability

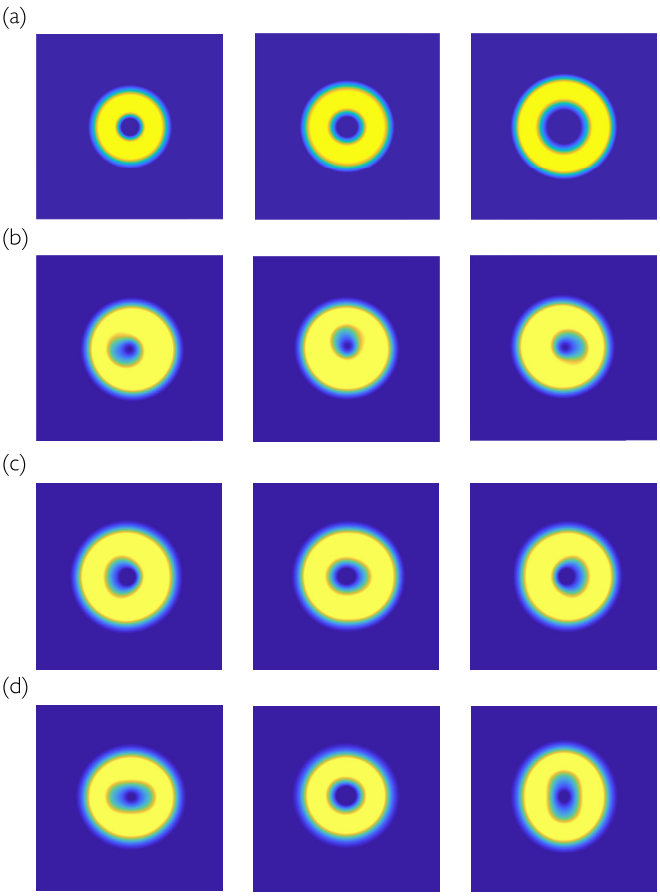

FIG. 11. Ring breathers and rotors in the E-I neural field resulting from destabilization of a stationary ring solution via Hopf bifurcation with respect to different eigenmodes: (a) destabilization of the $n = 0$ mode leading to an expanding contracting, radially symmetric ring breather; (b) destabilization of the $n = 1$ mode in a Hopf bifurcation to a onefold ring rotor or rotating solution with Z_1 rotational symmetry; (c) destabilization of the $n = 1$ mode in a Hopf bifurcation to a onefold expanding-contracting ring breather with D_1 dihedral symmetry across a single axis at all times; (d) destabilization of the $n = 2$ mode in a Hopf bifurcation leading to a twofold expanding contracting ring breather with D_2 dihedral symmetry across two axes at all times.

and Hopf bifurcation of stationary bump solutions was analyzed and presented in a notation permitting direct comparison of the structure and dependency on model parameters across this family of neural fields. We also obtain conditions that clarify when the *in-phase* and *antiphase* eigenmodes destabilize in the bifurcation and how it relates to the network parameters. To facilitate the existence and stability analysis of stationary bumps across this family of neural fields, a general vectorized neural field model to analyze any configuration of N interacting neural fields with M linear gating variables was established to analyze the general case.

Stationary bumps and their Hopf bifurcation on one-dimensional domain $(-\infty, \infty)$ are treated separately as there are significant differences in the model equations, its analysis, the structure of solutions and their bifurcations. An analogy may be drawn between the even-symmetric sum mode $\oplus$ on $\mathbb{R}$ and the case $n = 0$ on $\mathbb{R}^2$. A breather bifurcating from the $n = 0$ mode on $\mathbb{R}^2$ will appear as an expanding-contracting breather on $\mathbb{R}$ if we restrict the solution to any line through the origin. An analogy may also be drawn between the odd-symmetric difference mode $\ominus$ on $\mathbb{R}$ and the case $n = 1$ on $\mathbb{R}^2$. An expanding-contracting breather or rotor bifurcating from the $n = 1$ mode on $\mathbb{R}^2$ will appear as a side-to-side slosher on $\mathbb{R}$ if we restrict the solution to the line of reflection symmetry through the origin in the case of a breather with D_1 symmetry or any line through the origin in the case of a rotor with Z_1 symmetry. Higher-order even and odd modes exhibit a related structure.

Analytical results for stability and Hopf bifurcation with O(2) symmetry of stationary bumps were compared with numerical simulations in all neural fields discussed in this paper. In particular, in the vicinity of the Hopf bifurcation point, the type of emergent solution in purported supercritical Hopf bifurcations was compared to expectations from theory which should lead to n-fold breathers (i.e., stationary waves with D_n dihedral symmetry) or n-fold rotors (i.e., rotating waves with Z_n rotational symmetry). It was further sought to properly classify the Hopf bifurcation and clarify our previous work [15,20] in which we found additional types of time-periodic solutions. Different forms of radial and angular perturbations of the bump-like initial conditions were used to probe the nonlinear dynamics of the neural fields in the vicinity of the stationary bump to more effectively vet the stability of the bump and identify the types of stable solutions that can be approached in the vicinity of Hopf bifurcation points in this infinite-dimensional dynamical system.

In all of the cases we carefully inspected, it was consistently found that, in the vicinity of Hopf bifurcation points that were purported to be supercritical, the emergent solutions were either of the form of an expanding-contracting n-fold breather with D_n symmetry or an n-fold rotor with Z_n symmetry, where, in the case of breathers, the axis of alignment of the breather varied with initial conditions. Moreover, in the case of interacting pairs of symmetric neural fields, the n-fold breathers and rotors could be *in-phase* or *antiphase* depending on whether the $\pm$ eigenmode destabilizes.

However, near a Hopf bifurcation point in some parameter regions it was possible to find other types of periodic or oscillatory solutions and even multiple coexistent periodic solutions, particularly in the presence of an input inhomogeneity. These spatiotemporal oscillations could take the form of rotors with a different lobe count than n corresponding to the mode undergoing the Hopf bifurcation. Another form the oscillations could take on is similar to a rotor but characterized instead by counterpropagating lobes that emerge and collide on the boundary of the activity bump as observed in Fig. 4 in Ref. [20]. One can imagine such a solution by taking an n-fold rotor and reflecting a subset of the lobes so they rotate in the opposite direction and collide (or emerge) at various points. We have sometimes referred to these time-periodic solutions as *swimmers* as they appeared to do the breaststroke when the counterpropagating lobes are symmetric across an axis and emerge from the bump (see Fig. 4 in Ref. [20] for reference). When these occur, multiple forms of such solutions can be approached via different initial perturbations for the same

parameter values. In the interacting pair of symmetric neural fields, an interesting type of solution well beyond a Hopf bifurcation was a pair of antidirectional rotors, where the rotor in neural field layer I rotated at the same rate but opposite direction as the rotor in neural field layer II. Consequently, the investigation and description of these additional types of time-periodic spatiotemporal behavior warrants a separate treatment.

This work highlights a family of elementary neural fields and the main implication is to understand how network interactions and symmetry lead to the spatiotemporal structure of spatially coherent time-periodic oscillations arising from Hopf bifurcation. Such bifurcations may occur more universally in a wide range of more complex and biologically relevant neural field models, given the universality of bifurcations in nonlinear dynamical systems. It is also important to understand how modeling choices may lead to symmetry breaking or preclude certain types of bifurcations. Additionally, the set of existence and stability results collected herein may serve to support different applications of bumps and breathers in related neural field models.

It may be possible to observe stationary and oscillatory bumps either in *in vitro* or *in vivo* experimental preparations using optogenetics and voltage sensitive dyes. Optogenetics could be used to generate the input inhomogeneity by continually stimulating neurons in a local patch of tissue and observing the activity across a layer of the cortex with populations of neurons that form *short-range* synaptic connections that are approximately homogeneous and isotropic (distance-dependent). Different pharmacological conditions in *in vitro* slice preparations could be used to modify the properties of the network to observe the changes in the spatiotemporal behavior. Two densely interconnected areas with reciprocal and topographic connections, e.g., somatosensory cortices S1 and S2 [83], could be investigated by stimulating local patches of tissue in one or both regions and monitoring the activity in both. While it would be difficult to predict when such solutions should occur, our work suggests that one could expect at least two characteristic forms of *localized* spatiotemporal activity patterns as a steady-state response to a persistent localized input inhomogeneity in the form of a stationary activity bump of steady persistent activity or a stationary activity bump exhibiting spatiotemporal oscillations in the activity. We have also found the localized oscillations can emit an outward propagating circular wave, ring waves, and target patterns in response to an input in the AE neural field [15] and in some cases with inhibition when the network supports such waves in the absence of an input, indicating other types of responses one might observe that are not localized in space. Such waves perhaps might be observed, for example, in disinhibited cortical slice preparations that support wave propagation.

[1] H. Wilson and J. D. Cowan, A mathematical theory of the functional dynamics of cortical and thalamic nervous tissue, Biol. Cybern. **13**, 55 (1973).

[2] S.-I. Amari, Dynamics of pattern formation in lateral-inhibition type neural fields, Biol. Cybern. **27**, 77 (1977).

[3] D. J. Pinto, Computational, experimental, and analytic explorations of neuronal circuits in the cerebral cortex, Ph.D. thesis, University of Pittsburgh, 1997.

[4] G. B. Ermentrout, Neural networks as spatio-temporal pattern-forming systems, Rep. Prog. Phys. **61**, 353 (1998).

[5] J. G. Taylor, Neural 'bubble' dynamics in two dimensions: Foundations, Biol. Cybern. **80**, 393 (1999).

[6] H. Werner and T. Richter, Circular stationary solutions in two-dimensional neural fields, Biol. Cybern. **85**, 211 (2001).

[7] D. J. Pinto and G. B. Ermentrout, Spatially structured activity in synaptically coupled neuronal networks: I. Traveling fronts and pulses, SIAM J. Appl. Math. **62**, 206 (2001).

[8] D. J. Pinto and G. B. Ermentrout, Spatially structured activity in synaptically coupled neuronal networks: II. Lateral inhibition and standing pulses, SIAM J. Appl. Math. **62**, 226 (2001).

[9] C. Laing, W. C. Troy, B. S. Gutkin, and G. B. Ermentrout, Multiple bumps in a neuronal model of working memory, SIAM J. Appl. Math. **63**, 62 (2002).

[10] X. Xie, R. Hahnloser, and H. Seung, Double-ring network model of the head-direction system, Phys. Rev. E **66**, 041902 (2002).

[11] P. C. Bressloff, S. E. Folias, A. Prat, and Y.-X. Li, Oscillatory waves in inhomogeneous neural media, Phys. Rev. Lett. **91**, 178101 (2003).

[12] C. Laing and W. C. Troy, PDE methods for nonlocal models, SIAM J. Appl. Dyn. Syst. **2**, 487 (2003).

[13] C. Laing and W. C. Troy, Two-bump solutions of Amari-type models of neuronal pattern formation, Physica D **178**, 190 (2003).

[14] L. Zhang, On stability of traveling wave solutions in synaptically coupled neuronal networks, Differ. Integral Equ. **16**, 513 (2003).

[15] S. E. Folias and P. C. Bressloff, Breathing pulses in an excitatory neural network, SIAM J. Appl. Dyn. Syst. **3**, 378 (2004).

[16] J. E. Rubin and W. C. Troy, Sustained spatial patterns of activity in neuronal populations without recurrent excitation, SIAM J. Appl. Math. **64**, 1609 (2004).

[17] X. Huang, W. C. Troy, Q. Yang, H. Ma, C. R. Laing, S. J. Schiff, and J.-Y. Wu, Spiral waves in disinhibited mammalian neocortex, J. Neurosci. **24**, 9897 (2004).

[18] S. Coombes and M. Owen, Evans functions for integral neural field equations with Heaviside firing rate function, SIAM J. Appl. Dyn. Syst. **3**, 574 (2004).

[19] P. Blomquist, J. Wyller, and G. Einevoll, Localized activity patterns in two-population neuronal networks, Physica D **206**, 180 (2005).

[20] S. E. Folias and P. C. Bressloff, Breathers in two-dimensional neural media, Phys. Rev. Lett. **95**, 208107 (2005).

[21] C. Laing, Spiral waves in nonlocal equations, SIAM J. Appl. Dyn. Syst. **4**, 588 (2005).

[22] W. C. Troy and V. Shusterman, Patterns and features of families of traveling waves in large-scale neuronal networks, SIAM J. Appl. Dyn. Syst. **6**, 263 (2007).

[23] M. Owen, C. Laing, and S. Coombes, Bumps and rings in a two-dimensional neural field: Splitting and rotational instabilities, New J. Phys. **9**, 378 (2007).
[24] W. C. Troy, Wave phenomena in neuronal networks, in *Dissipative Solitons: From Optics to Biology and Medicine*, Lecture Notes in Physics Vol. 751 (Springer, Berlin, Heidelbrg, 2008), pp. 431–452.
[25] D. Pinto and W. C. Troy (unpublished).
[26] V. Shusterman and W. C. Troy, From baseline to epileptiform activity: A path to synchronized rhythmicity in large-scale neural networks, Phys. Rev. E **77**, 061911 (2008).
[27] A. Hutt and N. P. Rougier, Activity spread and breathers induced by finite transmission speeds in two-dimensional neural fields, Phys. Rev. E **82**, 055701(R) (2010).
[28] Z. P. Kilpatrick and P. C. Bressloff, Spatially structured oscillations in a two-dimensional excitatory neuronal network with synaptic depression, J. Comput. Neurosci. **28**, 193 (2010).
[29] P. C. Bressloff and Z. P. Kilpatrick, Two–dimensional bumps in piecewise smooth neural fields with synaptic depression, SIAM J. Appl. Math. **71**, 379 (2011).
[30] Y. Lu, Y. Sato, and S.-I. Amari, Traveling bumps and their collisions in a two-dimensional neural field, Neural Comput. **23**, 1248 (2011).
[31] S. E. Folias, Nonlinear analysis of breathing pulses in a synaptically coupled neural network, SIAM J. Appl. Dyn. Syst. **10**, 744 (2011).
[32] S. E. Folias and G. B. Ermentrout, New patterns of activity in a pair of interacting excitatory-inhibitory neural fields, Phys. Rev. Lett. **107**, 228103 (2011).
[33] S. E. Folias and G. B. Ermentrout, Bifurcations of stationary solutions in an interacting pair of E-I neural fields, SIAM J. Appl. Dyn. Syst. **11**, 895 (2012).
[34] S. Coombes, H. Schmidt, and I. Bojak, Interface dynamics in planar neural field models, J. Math. Neurosci. **2**, 9 (2012).
[35] P. C. Bressloff and S. Coombes, Neural 'bubble' dynamics revisited, Cogn. Comput. **5**, 281 (2013).
[36] G. Faye and J. Touboul, Pulsatile localized dynamics in delayed neural field equations in arbitrary dimension, SIAM J. Appl. Math. **74**, 1657 (2014).
[37] P. C. Bressloff, *Waves in Neural Media*, Lecture Notes on Mathematical Modeling in the Life Sciences (Springer Verlag, New York, NY, 2014).
[38] G. B. Ermentrout, S. E. Folias, and Z. P. Kilpatrick, Spatiotemporal pattern formation in neural fields with linear adaptation, in *Neural Fields*, edited by S. Coombes, P. beim Graben, R. Potthast, and J. Wright (Springer, Heidelberg, 2014), pp. 119–151.
[39] S. ichi Amari, Heaviside world: Excitation and self-organization of neural fields, in *Neural Fields*, edited by S. Coombes, P. beim Graben, R. Potthast, and J. Wright (Springer, Heidelberg, 2014), pp. 97–118.
[40] S. Coombes, H. Schmidt, and D. Avitabile, Spots: Breathing, drifting and scattering in a neural field model, in *Neural Fields*, edited by S. Coombes, P. beim Graben, R. Potthast, and J. Wright (Springer, Heidelberg, 2014), pp. 187–214.
[41] C. R. Laing, PDE methods for two-dimensional neural fields, in *Neural Fields*, edited by S. Coombes, P. beim Graben, R. Potthast, and J. Wright (Springer, Heidelberg, 2014), pp. 153–174.
[42] Z. P. Kilpatrick and P. C. Bressloff, Stochastic motion of bumps in planar neural fields, SIAM J. Appl. Math. **75**, 1553 (2015).
[43] E. Burlakov, J. Wyller, and A. Ponosov, Two-dimensional amari neural field model with periodic microstructure: Rotationally symmetric bump solutions, Commun. Nonlin. Sci. Numer. Simul. **32**, 81 (2016).
[44] A. Gökçe, D. Avitabile, and S. Coombes, The dynamics of neural fields on bounded domains: An interface approach for dirichlet boundary conditions, J. Math. Neurosci. **62**, 226 (2017).
[45] G. Deco, V. K. Jirsa, P. A. Robinson, M. Breakspear, and K. Friston, The dynamic brain: From spiking neurons to neural masses and cortical fields, PLoS Comput. Biol. **4**, e1000092 (2008).
[46] J.-Y. Wu, L. Guan, and Y. Tsau, Propagating activation during oscillations and evoked responses in neocortical slices, J. Neurosci. **19**, 5005 (1999).
[47] J.-Y. Wu, L. Guan, L. Bai, and Q. Yang, Spatiotemporal properties of an evoked population activity in rat sensory cortical slices, J. Neurophysiol. **86**, 2461 (2001).
[48] J.-Y. Wu, X. Huang, and C. Zhang, Propagating waves of activity in the neocortex: What they are, what they do, Neuroscientist **14**, 487 (2008).
[49] Y. Xiao, X.-Y. Huang, S. Van Wert, E. Barreto, J.-Y. Wu, B. J. Gluckman, and S. J. Schiff, The role of inhibition in oscillatory wave dynamics in the cortex, Eur. J. Neurosci. **36**, 2201 (2012).
[50] W. Xu, X. Huang, K. Takagaki, and J.-Y. Wu, Compression and reflection of visually evoked cortical waves, Neuron **55**, 119 (2007).
[51] Z. Yang, D. J. Heeger, R. Blake, and E. Seidemann, Long-range traveling waves of activity triggered by local dichoptic stimulation in V1 of behaving monkeys, J. Neurophysiol. **113**, 277 (2015).
[52] J. W. Yang, S. An, J. J. Sun, and V. Reyes-Puerta, Thalamic network oscillations synchronize ontogenetic columns in the newborn rat barrel cortex, Cereb. Cortex **23**, 1299 (2013).
[53] K. Takagaki, C. Zhang, J.-Y. Wu, and M. T. Lippert, Cross-modal propagation of sensory-evoked and spontaneous activity in the rat neocortex, Neurosci. Lett. **431**, 191 (2008).
[54] T. P. Zanos, P. J. Mineault, K. T. Nasiotis, and D. Guitton, A sensorimotor role for traveling waves in primate visual cortex, Neuron **85**, 615 (2015).
[55] H. Zhang and J. Jacobs, Traveling theta waves in the human hippocampus, J. Neurosci. **35**, 12477 (2015).
[56] T. Berger, A. Borgdorff, S. Crochet, F. B. Neubauer, S. Lefort, B. Fauvet, I. Ferezou, A. Carleton, H. R. Lüscher, and C. C. H. Petersen, Combined voltage and Calcium epifluorescence imaging *in vitro* and *in vivo* reveals subthreshold and suprathreshold dynamics of mouse barrel cortex, J. Neurophysiol. **97**, 3751 (2007).
[57] Y. Chagnac-Amitai and B. W. Connors, Horizontal spread of synchronized activity in neocortex and its control by gaba-mediated inhibition, J. Neurophysiol. **61**, 747 (1989).
[58] R. B. Langdon and M. Sur, Components of field potentials evoked by white matter stimulation in isolated slices of primary visual cortex: Spatial distributions and synaptic order, J. Neurophysiol. **64**, 1484 (1990).
[59] I. Nauhaus, L. Busse, D. L. Ringach, and M. Carandini, Robustness of traveling waves in ongoing activity of visual cortex, J. Neurosci. **32**, 3088 (2012).

[60] D. J. Pinto, S. Patrick, W. Huang, and B. Connors, Initiation, propagation, and termination of epileptiform activity in rodent neocortex *in vitro* involve distinct mechanisms, J. Neurosci. **25**, 8131 (2005).

[61] W. Xu, B. S. Wolff, and J.-Y. Wu, Low-intensity electric fields induce two distinct response components in neocortical neuronal populations, J. Neurophysiol. **112**, 2446 (2014).

[62] L. Muller and A. Destexhe, Propagating waves in thalamus, cortex and the thalamocortical system: Experiments and models, J. Physiol. Paris **106**, 222 (2012).

[63] D. Contreras and R. Llinás, Voltage-Sensitive dye imaging of neocortical spatiotemporal dynamics to afferent activation frequency, J. Neurosci. **21**, 9403 (2001).

[64] T. Sato, I. Nauhaus, and M. Carandini, Traveling waves in visual cortex, Neuron **75**, 218 (2012).

[65] K. A. Richardson, S. J. Schiff, and B. J. Gluckman, Control of traveling waves in the mammalian cortex, Phys. Rev. Lett. **94**, 028103 (2005).

[66] A. Benucci, R. A. Frazor, and M. Carandini, Standing waves and traveling waves distinguish two circuits in visual cortex, Neuron **55**, 103 (2007).

[67] S. Hubatz, G. Hucher, D. E. Shulz, and I. Férézou, Spatiotemporal properties of whisker-evoked tactile responses in the mouse secondary somatosensory cortex, Sci. Rep. **10**, 763 (2020).

[68] X. Geng and J.-Y. Wu, 'Blue' voltage-sensitive dyes for studying spatiotemporal dynamics in the brain: Visualizing cortical waves, Neurophotonics **4**, 031207 (2017).

[69] T. D. Fehérvári, Y. Okazaki, H. Sawai, and T. Yagi, *In vivo* voltage-sensitive dye study of lateral spreading of cortical activity in mouse primary visual cortex induced by a current impulse, PLoS ONE **10**, e0133853 (2015).

[70] B. R. Lustig, R. M. Friedman, J. E. Winberry, F. F. Ebner, and A. W. Roe, Voltage-sensitive dye imaging reveals shifting spatiotemporal spread of whisker-induced activity in rat barrel cortex, J. Neurophysiol. **109**, 2382 (2013).

[71] S. Chemla and F. Chavane, Effects of GABAA kinetics on cortical population activity: Computational studies and physiological confirmations, J. Neurophysiol. **115**, 2867 (2016).

[72] X. Huang, W. Xu, L. Jianmin, K. Takagaki, X. Gao, and J.-Y. Wu, Spiral wave dynamics in neocortex, Neuron **65**, 978 (2010).

[73] M. Lippert, K. Takagaki, W. Xu, X. Huang, and J.-Y. Wu, Methods for voltage-sensitive dye imaging of rat cortical activity with high signal-to-noise ratio, J. Neurophysiol. **98**, 502 (2007).

[74] L. Muller, A. Reynaud, F. Chavane, and A. Destexhe, The stimulus-evoked population response in visual cortex of awake monkey is a propagating wave, Nat. Commun. **5**, 3675 (2014).

[75] Y. Chen, C. R. Palmer, and E. Seidemann, The relationship between voltage-sensitive dye imaging signals and spiking activity of neural populations in primate v1, J. Neurophysiol. **107**, 3281 (2012).

[76] I. Férézou, S. Bolea, and C. C. H. Petersen, Visualizing the cortical representation of whisker touch: Voltage-Sensitive dye imaging in freely moving mice, Neuron **50**, 617 (2006).

[77] D. Shoham, D. E. Glaser, A. Arieli, T. Kenet, C. Wijnbergen, Y. Toledo, R. Hildesheim, and A. Grinvald, Imaging cortical dynamics at high spatial and temporal resolution with novel blue voltage-sensitive dyes, Neuron **24**, 791 (1999).

[78] Q. Yu, X. Wang, and L. Nie, Optical recording of brain functions based on voltage-sensitive dyes, Chin. Chem. Lett. **32**, 1879 (2021).

[79] K. Wimmer, D. Q. Nykamp, C. Constantinidis, and A. Compte, Bump attractor dynamics in prefrontal cortex explains behavioral precision in spatial working memory, Nat. Neurosci. **17**, 431 (2014).

[80] G. N. Watson, *A Treatise on the Theory of Bessel Functions* (Cambridge University Press, Cambridge, UK, 1952).

[81] T. Kato, *Perturbation Theory for Linear Operators*, Classics in Mathematics (Springer Verlag, New York, 1966).

[82] M. Golubitsky and D. Schaeffer, *Singularities and Groups in Bifurcation Theory: Vol. II*, Applied Mathematical Sciences 69 (Springer Verlag, New York, NY, 1988).

[83] G. Minamisawa, S. E. Kwon, M. Chevée, S. P. Brown, and D. H. O'Connor, A non-canonical feedback circuit for rapid interactions between somatosensory cortices, Cell Rep. **23**, 2718 (2018).